Consistent Volumetric Search for Accurate Passive Coherent Location

Daniel P. Nicolalde-Rodríguez, *Student Member, IEEE,* Wallace A. Martins, *Senior Member, IEEE,* José A. Apolinário Jr., *Senior Member, IEEE,* and Marcello L. R. de Campos, *Senior Member, IEEE*.

***Abstract*—This paper addresses multiple-transmitter/receiver passive coherent location (PCL) system observing a single target with possible bistatic range mismeasurements (outliers) caused by non-line-of-sight effects. It proposes a unified mathematical framework for target location algorithms including spherical interpolation (SI), spherical intersection (SX), and nonlinearly constrained least squares (NLCLS), generalizing them for scenarios with multiple transmitters and receivers. While algorithms SI and SX employ closed-form expressions without considering all nonlinear relationships among the optimization variables, the NLCLS takes these nonlinearities into account via constraints; its simplified and faster version, with promising results and reduced computational burden, is also proposed. The Cramer-Rao lower bound is derived for this application. To handle outliers in a 3D PCL system, the paper proposes a volumetric search method that divides the search region into cuboids to select consistent bistatic range measurements, enabling accurate target location estimation. Additionally, the centroid of the selected cuboid provides an alternative location estimate. Another consistent approach to measurement selection is introduced for benchmarking, involving iterative removal of outliers based on comparisons of cost functions. Numerical experiments demonstrate the robustness of the proposed cuboid-based methods, particularly in scenarios with increased bistatic range mismeasurements.**

***Index Terms*—Passive coherent location, bistatic delays, bistatic range, measurement selection, outliers, cuboid.**

I. Introduction

PASSIVE coherent location systems, also known as passive radars, have attracted great interest, for they do not need exclusive transmitters (TXs) to detect, track, and locate targets of interest [1], [2]. Using sensors under the designer's control, also referred to herein as receivers (RXs), to acquire signals already available from TX systems, passive radar systems do not generate spectral congestion. Examples of these noncooperative illuminators of opportunity (IoO) signals are analog frequency modulation audio broadcaster (FM), digital audio broadcasting (DAB), digital video broadcaster-terrestrial (DVB-T), automatic identification system satellite (AIS-S), global positioning system (GPS), and mobile communication system (2G, 3G, 4G, 5G and beyond) [3]–[7].

PCL algorithms usually rely on accurate estimates of the *bistatic range* associated with each TX-RX pair. The bistatic range measurement can be obtained by multiplying the bistatic target delay measurement by the propagation speed [1], [8]. In a simple bistatic scenario (one TX, one RX, and one target), the bistatic target delay (the literature also refers to this delay as time-difference-of-arrival (TDoA), propagation delay, bistatic delay, time delay, etc.) represents the time difference between the IoO signal, emitted by TX and collected by the reference channel (RC) in the RX, and the target-reflected signal acquired by the surveillance channel (SC) in the same RX.

The authors in [1], [9]–[12] showed that bistatic range measurements in a multistatic (i.e., with multiple TXs/RXs) PCL scenario lead to accurate location estimations. In fact, many different PCL investigations have been conducted based on bistatic range measurements [10]–[21]. The literature, however, mainly deals with passive radar location solutions based on bistatic ranges for multiple TXs and one RX or multiple RXs and one TX. On the other hand, the work in [22] describes a least square (LS) solution of a passive location system based on time-sum-of-arrival (TSoA) measurements in a scenario of multiple TXs and multiple RXs. TSoA represents the travel time of the IoO signal emitted by the TX reflected in the target and collected by the SC in the RX. Nevertheless, a PCL formulation consisting of bistatic range measurements associated with multiple TXs and RXs remains unexplored.

This work extends the formulation of PCL algorithms using spherical interpolation (SI) and spherical intersection (SX), previously derived with multiple TXs and one RX scenario [12] as well as multiple RXs and one TX scenario [11], to the general case of a multistatic geometry with multiple TXs/RXs. We also propose the multiple TXs/RXs formulation of the nonlinearly constrained least squares algorithm, designed initially for multiple RXs and one TX [11], where we use all constraints to improve the accuracy of the original SI technique. In addition, the paper proposes a fast and simplified scheme (S-NLCLS) with a single constraint. S-NLCLS significantly reduces the computational load compared with the original NLCLS algorithm, while achieving similar results in terms of location accuracy. We also derive the Crámer-Rao lower bound (CRLB) for benchmarking the multistatic PCL location algorithms investigated herein.

Before obtaining bistatic measurements, one first needs to detect the target, usually using thresholds in the cross-correlation (CC) between the received RC and SC signals [1], [23]. These detectors perform well when the RC has low background noise and no external interference in the SC. More advanced target detection procedures in [24]–[27] overcome

D. P. Nicolalde-Rodríguez and M. L. R. de Campos are with the Electrical Engineering Program (PEE), COPPE / Federal University of Rio de Janeiro (UFRJ), Rio de Janeiro, RJ, Brazil (e-mails: danielnicolalde@gmail.com; campos@smt.ufrj.br).

W. A. Martins is with ISAE-SUPAERO, Université de Toulouse, 31055 Toulouse, France (e-mail: wallace.martins@isae-supaero.fr).

J. A. Apolinário Jr. is with the Department of Electrical Engineering, Military Institute of Engineering (IME), Rio de Janeiro, RJ, Brazil (e-mail: apolin@ime.eb.br).

adverse effects like noisy RC and direct path interference (DPI) in the SC. In a bistatic PCL scenario, the target echo in the SC can also be masked by clutter echoes generated by IoO signal reflections in dominated stationary objects (multipath zero-Doppler interference). Spatial and temporal adaptive filtering algorithms can be used to reduce such clutter and DPI interference [1], [28]–[33]. By using bistatic parameter-based expectation–maximization (EM) algorithms [19], one can jointly estimate target and clutter delays as well as Doppler frequencies of the targets while also eliminating DPI effects. We address herein the necessary modifications for the formulation of location algorithms when one or more delay measurements have not been detected.

However, we commonly find unreliable measurements, i.e., mismeasurements or outliers, among the bistatic range measurements due to non-line-of-sight (NLoS) between the TX and target or target and RX, or the presence of another target. Outliers generated by the existence of another target are out of the scope of this paper. Unlike clutter interference (zero-Doppler detectable interference), the NLoS effect is inevitable and could be masked in bistatic target measurements. NLoS interference creates biased measurements due to the affected blocked signal path, which becomes longer than usual [28].

Recent works [22], [34]–[36] have tackled mismeasurements produced by NLoS effect in 2D passive elliptic location systems with one target. The work in [22] proposes two LS data-selective techniques. The first technique uses different combinations of measurements to compare cost functions and select consistent measurements. The second technique follows ellipsoid parameterization to select data. The authors in [34] used an augmented Lagrange programming neural network (ALPNN) to balance the parameters in the traditional LS formulation. The proposal in [35] suggests completing a resistant outlier matrix that contains measurements rather than using consistent data, using a constrained minimization loss function. The authors in [36] proposed a robust estimator that uses a differentiable error measure that overcomes the presence of outliers. This paper proposes two techniques to overcome outliers in 3D PCL systems.

Our first proposal is a region-based search algorithm that selects consistent bistatic measurements and offers a direct target location estimate. Our proposed technique splits the location region into cuboids. The cuboid associated with most measurements is considered to be the one that potentially contains the target location and is therefore employed to separate consistent data from mismeasurements. Moreover, the centroid of the referred cuboid can be considered a new target estimate. As seen in Section V, this proposed target location estimation shows promising results in terms of accuracy. Our proposal was motivated by the works in [37] and [38] that suggest cuboid-based search algorithms that select consistent time-difference-of-flight (TDoF)/time-of-flight (ToF) measurements for acoustic sensor location. Considering that a region of constant TDoF is a hyperboloid of two sheets with foci located at two loudspeakers, the problem could be seen as selecting the cuboid that intersects most hyperboloids associated with the different pairs of loudspeakers. We extend this criterion to PCL, where the selected cuboid intersects most ellipsoids associated with most target delay measurements collected from the different TX/RX pairs.

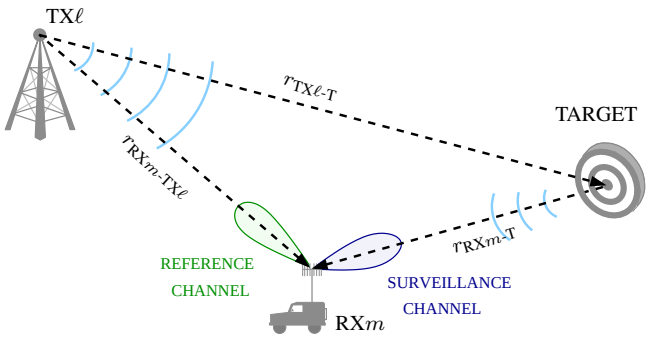

Fig. 1. Geometry of a passive coherent location system.

For benchmarking, we also propose a selection method for PCL that iteratively discards mismeasurements (one by one) of a candidate list. A cost function determines the bistatic measurement that must be discarded at each iteration. The iterative process stops automatically when all the selected bistatic measurement errors are below a predefined threshold. We find similar approaches in [22], [39]–[41]. The works in [39] and [22] select TDoAs in an emitting source and TSoAs in a passive location system, respectively. They define a fixed number of selected data, and the data set that obtains the least cost is employed to compute the final location. On the other hand, an iterative procedure in [40], [41] removes one-by-one time delay estimates (TDEs) associated with a pair of acoustic sensors in a scenario that detects the direction-of-arrival (DoA) of gunshots. The algorithm's stopping criterion also depends on a fixed number of selected data.

The organization of this paper is as follows. Section II describes the mathematical formulation of PCL algorithms (SI, SX, and NLCLS/S-NLCLS) in a multiple TXs/RXs scenario. Section III addresses the proposed techniques to overcome outliers. Section IV details the adaptation that must be carried out in the location algorithm when applying data selection. Section V presents the experimental results obtained from simulations. Finally, conclusions are stated in Section VI.

II. Location Algorithms

We assume a multistatic PCL geometry with M RXs and L noncooperative TXs that illuminate the target region, denoted as RXm, $m \in \mathcal{M} \triangleq \{1, 2, \ldots, M\}$, and TX$\ell$, $\ell \in \mathcal{L} \triangleq \{1, 2, \ldots, L\}$, respectively. Fig. 1 sketches the bistatic PCL geometry of the pair RXm-TXℓ. Vectors $\mathbf{p}_{\mathrm{RX}m}$ and $\mathbf{p}_{\mathrm{TX}\ell}$ represent the known positions of RXm and TXℓ, respectively. The unknown location of the target is represented by vector $\mathbf{p}_{\mathrm{T}}$ in an N-dimension problem, $N \in \{2, 3\}$.[1]

As shown in Fig. 1, the distances of interest in the PCL scenario are defined as: $r_{\mathrm{TX}\ell\text{-T}} \triangleq \|\mathbf{p}_{\mathrm{TX}\ell} - \mathbf{p}_{\mathrm{T}}\|$ (TXℓ–target range), $r_{\mathrm{RX}m\text{-T}} \triangleq \|\mathbf{p}_{\mathrm{RX}m} - \mathbf{p}_{\mathrm{T}}\|$ (RXm–target range), and $r_{\mathrm{RX}m\text{-TX}\ell} \triangleq \|\mathbf{p}_{\mathrm{RX}m} - \mathbf{p}_{\mathrm{TX}\ell}\|$ (RXm–TXℓ range).

The bistatic range $r_{\mathrm{B}m\ell}$ associated with each TXℓ-RXm pair represents the difference between the path length of the

[1]For the forthcoming explanations, we consider here the more general case where $N = 3$.

reflected signal in the target ($r_{\mathrm{RX}m\text{-T}} + r_{\mathrm{TX}\ell\text{-T}}$) and the line-of-sight path length ($r_{\mathrm{RX}m\text{-TX}\ell}$) [1], [8], i.e.

$$r_{\mathrm{B}m\ell} \triangleq r_{\mathrm{RX}m\text{-T}} + r_{\mathrm{TX}\ell\text{-T}} - r_{\mathrm{RX}m\text{-TX}\ell}. \quad (1)$$

The reflected path length associated with each TXℓ-RXm pair, known as range difference $r_{m\ell}$, is defined as

$$r_{m\ell} \triangleq r_{\mathrm{RX}m\text{-T}} + r_{\mathrm{TX}\ell\text{-T}}, \quad (2)$$

which can also be expressed as $r_{m\ell} = r_{\mathrm{B}m\ell} + r_{\mathrm{RX}m\text{-TX}\ell}$. Eq. (2) is the basis of the PCL approach for multiple TXs/RXs, and from it, we write

$$\left(r_{m\ell} - r_{\mathrm{TX}\ell\text{-T}}\right)^2 = r^2_{\mathrm{RX}m\text{-T}}, \quad (3)$$

which is the second-degree equation used to formulate the PCL problem when the number of RXs is larger than the number of TXs, i.e., when $M \geq L$. In case $L \geq M$, one can use $\left(r_{m\ell} - r_{\mathrm{RX}m\text{-T}}\right)^2 = r^2_{\mathrm{TX}\ell\text{-T}}$ instead. We assume $M \geq L$ in the forthcoming derivations for conciseness.

Eq. (3) can be rewritten as

$$\bar{\mathbf{p}}^{\intercal}_{\mathrm{RX}m\text{-TX}\ell}\bar{\mathbf{p}}_{\mathrm{T\text{-}TX}\ell} - r_{m\ell}r_{\mathrm{TX}\ell\text{-T}} = \frac{1}{2}(r^2_{\mathrm{RX}m\text{-TX}\ell} - r^2_{m\ell}), \quad (4)$$

in which $\bar{\mathbf{p}}_{\mathrm{RX}m\text{-TX}\ell} \triangleq \mathbf{p}_{\mathrm{RX}m} - \mathbf{p}_{\mathrm{TX}\ell}$ and $\bar{\mathbf{p}}_{\mathrm{T\text{-}TX}\ell} \triangleq \mathbf{p}_{\mathrm{T}} - \mathbf{p}_{\mathrm{TX}\ell}$. The unknown variables $\bar{\mathbf{p}}_{\mathrm{T\text{-}TX}\ell}$ and $r_{\mathrm{TX}\ell\text{-T}}$ must be computed to estimate the target location.

For our PCL system with M RXs, L TXs, and one target, we define the $ML \times NL$ block-diagonal matrix $\mathbf{P}_{\mathrm{RX\text{-}TX}} \triangleq \mathrm{diag}\left\{\bar{\mathbf{P}}_{\mathrm{RX\text{-}TX}\ell}\right\}_{\ell\in\mathcal{L}}$, where the m-th row of the $M \times N$ matrix $\bar{\mathbf{P}}_{\mathrm{RX\text{-}TX}\ell}$ is $\bar{\mathbf{p}}^{\intercal}_{\mathrm{RX}m\text{-TX}\ell}$. The $ML \times L$ block-diagonal matrix $\mathbf{R} \triangleq \mathrm{diag}\left\{\mathbf{r}_\ell\right\}_{\ell\in\mathcal{L}}$ is also defined, where the m-th entry of the $M \times 1$ vector $\mathbf{r}_\ell$ is $r_{m\ell}$. Moreover, we define $\bar{\mathbf{p}}_{\mathrm{T\text{-}TX}} \triangleq \left[\bar{\mathbf{p}}^{\intercal}_{\mathrm{T\text{-}TX}1}\cdots\bar{\mathbf{p}}^{\intercal}_{\mathrm{T\text{-}TX}L}\right]^{\intercal}$, $\mathbf{r}_{\mathrm{TX\text{-}T}} \triangleq \left[r_{\mathrm{TX}1\text{-T}}\ldots r_{\mathrm{TX}L\text{-T}}\right]^{\intercal}$, and $\mathbf{z} \triangleq \left[\mathbf{z}^{\intercal}_1\ldots\mathbf{z}^{\intercal}_L\right]^{\intercal}$, where $\mathbf{z}_\ell = \left[z_{1\ell}\ldots z_{M\ell}\right]^{\intercal}$, and $z_{m\ell} = \frac{1}{2}\left(r^2_{\mathrm{RX}m\text{-TX}\ell} - r^2_{m\ell}\right)$.

Expanding Eq. (4) for M RXs and L TXs, we have

$$\mathbf{P}_{\mathrm{RX\text{-}TX}}\bar{\mathbf{p}}_{\mathrm{T\text{-}TX}} - \mathbf{R}\mathbf{r}_{\mathrm{TX\text{-}T}} = \mathbf{z}. \quad (5)$$

Associating the known matrix $\mathbf{A} \triangleq \begin{bmatrix}\mathbf{P}_{\mathrm{RX\text{-}TX}} & -\mathbf{R}\end{bmatrix}$ and the unknown vector $\mathbf{x} \triangleq \begin{bmatrix}\bar{\mathbf{p}}^{\intercal}_{\mathrm{T\text{-}TX}} & \mathbf{r}^{\intercal}_{\mathrm{TX\text{-}T}}\end{bmatrix}^{\intercal}$, Eq. (5) leads to

$$\mathbf{A}\mathbf{x} = \mathbf{z}. \quad (6)$$

The entries of $\mathbf{x}$ are nonlinearly related since $\mathbf{r}_{\mathrm{TX\text{-}T}}$ is a (known) nonlinear function of $\bar{\mathbf{p}}_{\mathrm{T\text{-}TX}}$, which makes Eq. (6) a nonlinear equation on $\bar{\mathbf{p}}_{\mathrm{T\text{-}TX}}$. In order to estimate $\mathbf{x}$, $\hat{\mathbf{x}}$, we employ practical bistatic measurements to obtain estimated versions of matrix $\mathbf{A}$ and vector $\mathbf{z}$; formally, $\hat{\mathbf{A}}$ and vector $\hat{\mathbf{z}}$. $\hat{\mathbf{A}}$ and $\hat{\mathbf{z}}$ are not necessarily related as in Eq. (6). To simplify our notation, we use the original notation, $\mathbf{A}$ and $\mathbf{z}$, for the forthcoming mathematical formulations.

To estimate the target location, one usually searches for the $\mathbf{x}$ vector ($\hat{\bar{\mathbf{p}}}_{\mathrm{T\text{-}TX}}$ and $\hat{\mathbf{r}}_{\mathrm{TX\text{-}T}}$), that minimizes some model mismatch metric (e.g., the squared norm of the error vector $\mathbf{e} \triangleq \mathbf{A}\mathbf{x} - \mathbf{z}$).

Following [12], two classical methods approximate the solution $\bar{\mathbf{p}}_{\mathrm{T\text{-}TX}}$ that minimizes the squared norm of $\mathbf{e}$, namely: SI and SX. The application of the two methods to the case of multiple TXs and one RX is addressed in [12], and to the scenario of multiple RXs and one TX is addressed in [11]. In the following, we extend the mathematical formulations of the two methods to the generic case of multiple TXs and RXs.

A. Spherical Interpolation

The model mismatch in Eq. (6) when employing bistatic measurements can be approached using the unconstrained LS solution, which is obtained by equating the gradient of the LS cost function $\xi(\mathbf{x})$ to the null vector, i.e., $\nabla_{\mathbf{x}}\xi(\mathbf{x}) = \mathbf{0}$, where

$$\xi(\mathbf{x}) \triangleq \mathbf{e}^{\intercal}\mathbf{e}. \quad (7)$$

Thus, knowing that $\mathbf{A}$ is $ML \times (N+1)L$, a necessary condition for $\mathbf{A}^{\intercal}\mathbf{A}$ to be invertible is $M \geq N+1$, i.e., the number of receivers must be larger than the problem dimension (2D or 3D); in that case, the unconstrained LS solution becomes

$$\hat{\mathbf{x}} = \left(\mathbf{A}^{\intercal}\mathbf{A}\right)^{-1}\mathbf{A}^{\intercal}\mathbf{z} = \begin{bmatrix}\hat{\bar{\mathbf{p}}}^{\intercal}_{\mathrm{T\text{-}TX}} & \hat{\mathbf{r}}^{\intercal}_{\mathrm{TX\text{-}T}}\end{bmatrix}^{\intercal}. \quad (8)$$

Note that $\hat{\bar{\mathbf{p}}}_{\mathrm{T\text{-}TX}}$ corresponds to the first NL elements of $\hat{\mathbf{x}}$. Since we can express $\bar{\mathbf{p}}_{\mathrm{T\text{-}TX}}$ as

$$\underbrace{\begin{bmatrix}\mathbf{p}_{\mathrm{T}} - \mathbf{p}_{\mathrm{TX}1}\\ \vdots \\ \mathbf{p}_{\mathrm{T}} - \mathbf{p}_{\mathrm{TX}L}\end{bmatrix}}_{\bar{\mathbf{p}}_{\mathrm{T\text{-}TX}}} = \underbrace{\begin{bmatrix}\mathbf{I}_{N\times N}\\ \vdots \\ \mathbf{I}_{N\times N}\end{bmatrix}}_{\mathbf{I}_{\mathrm{a}}}\mathbf{p}_{\mathrm{T}} - \underbrace{\begin{bmatrix}\mathbf{p}_{\mathrm{TX}1}\\ \vdots \\ \mathbf{p}_{\mathrm{TX}L}\end{bmatrix}}_{\mathbf{p}_{\mathrm{TX}}}, \quad (9)$$

we expect to have $\hat{\bar{\mathbf{p}}}_{\mathrm{T\text{-}TX}} \approx \mathbf{I}_{\mathrm{a}}\mathbf{p}_{\mathrm{T}} - \mathbf{p}_{\mathrm{TX}}$, and therefore the final estimate of $\mathbf{p}_{\mathrm{T}}$ is computed as

$$\hat{\mathbf{p}}_{\mathrm{T}} = \left(\mathbf{I}_{\mathrm{a}}{}^{\intercal}\mathbf{I}_{\mathrm{a}}\right)^{-1}\mathbf{I}_{\mathrm{a}}{}^{\intercal}\left(\hat{\bar{\mathbf{p}}}_{\mathrm{T\text{-}TX}} + \mathbf{p}_{\mathrm{TX}}\right), \quad (10)$$

which represents the mean of L individual estimates for each case of 1 TX and M RXs: $\hat{\mathbf{p}}_{\mathrm{T}} = \frac{1}{L}\sum_{\ell=1}^{L}\left(\hat{\bar{\mathbf{p}}}_{\mathrm{T\text{-}TX}\ell} + \mathbf{p}_{\mathrm{TX}\ell}\right)$.

B. Spherical Intersection

From Eq. (5), we can estimate $\bar{\mathbf{p}}_{\mathrm{T\text{-}TX}}$ as

$$\hat{\bar{\mathbf{p}}}_{\mathrm{T\text{-}TX}} = \mathbf{P}^{\dagger}\left(\mathbf{z} + \mathbf{R}\mathbf{r}_{\mathrm{TX\text{-}T}}\right), \quad (11)$$

where $\mathbf{P}^{\dagger} = \left(\mathbf{P}^{\intercal}_{\mathrm{RX\text{-}TX}}\mathbf{P}_{\mathrm{RX\text{-}TX}}\right)^{-1}\mathbf{P}^{\intercal}_{\mathrm{RX\text{-}TX}}$ and, in this case, a necessary condition for $\mathbf{P}^{\intercal}_{\mathrm{RX\text{-}TX}}\mathbf{P}_{\mathrm{RX\text{-}TX}}$ to be invertible is $M \geq N$. Eq. (11) can be compactly expressed as

$$\hat{\bar{\mathbf{p}}}_{\mathrm{T\text{-}TX}} = \mathbf{a} + \mathbf{B}\mathbf{r}_{\mathrm{TX\text{-}T}}, \quad (12)$$

where $\mathbf{a} \triangleq \mathbf{P}^{\dagger}\mathbf{z}$ and $\mathbf{B} \triangleq \mathbf{P}^{\dagger}\mathbf{R}$. Considering the block-diagonal structure of matrix $\mathbf{P}_{\mathrm{RX\text{-}TX}}$, we can write $\mathbf{P}^{\dagger} = \mathrm{diag}\left\{\mathbf{P}^{\dagger}_{\ell}\right\}_{\ell\in\mathcal{L}}$, thus allowing us to rewrite the $LN \times 1$ vector $\mathbf{a}$ in Eq. (12) as $\mathbf{a} = \left[\mathbf{a}^{\intercal}_1\ldots\mathbf{a}^{\intercal}_L\right]^{\intercal}$, and the $NL \times L$ block-diagonal matrix $\mathbf{B} = \mathrm{diag}\left\{\mathbf{b}_\ell\right\}_{\ell\in\mathcal{L}}$, where $\mathbf{a}_\ell = \mathbf{P}^{\dagger}_{\ell}\mathbf{z}_\ell$ and $\mathbf{b}_\ell = \mathbf{P}^{\dagger}_{\ell}\mathbf{r}_\ell$ ($N \times 1$ vectors). Expanding Eq. (12), one has L relations as follows: $\hat{\bar{\mathbf{p}}}_{\mathrm{T\text{-}TX}\ell} = \mathbf{a}_\ell + \mathbf{b}_\ell r_{\mathrm{TX}\ell\text{-T}}, \forall\ell \in \mathcal{L}$.

We expect to have $r^2_{\mathrm{TX}\ell\text{-T}} \approx \|\hat{\bar{\mathbf{p}}}_{\mathrm{T\text{-}TX}\ell}\|^2$, such that $r^2_{\mathrm{TX}\ell\text{-T}} \approx \left(\mathbf{a}_\ell + \mathbf{b}_\ell r_{\mathrm{TX}\ell\text{-T}}\right)^{\intercal}\left(\mathbf{a}_\ell + \mathbf{b}_\ell r_{\mathrm{TX}\ell\text{-T}}\right)$. Therefore, the estimate of $r_{\mathrm{TX}\ell\text{-T}}$ can be seen as the solution of a simple quadratic equation: $\hat{r}_{\mathrm{TX}\ell\text{-T}} = \frac{-2\mathbf{a}^{\intercal}_\ell\mathbf{b}_\ell \pm \sqrt{4(\mathbf{a}^{\intercal}_\ell\mathbf{b}_\ell)^2 - 4(\mathbf{b}^{\intercal}_\ell\mathbf{b}_\ell - 1)\mathbf{a}^{\intercal}_\ell\mathbf{a}_\ell}}{2(\mathbf{b}^{\intercal}_\ell\mathbf{b}_\ell - 1)}$. Thus, there are two options for each $\hat{r}_{\mathrm{TX}\ell\text{-T}}$, $\ell \in \mathcal{L}$; therefore, we have 2^L possible estimates of vector $\mathbf{r}_{\mathrm{TX\text{-}T}}$ in total. All those estimates are evaluated in Eq. (11) to obtain the possible

vectors of $\hat{\bar{\mathbf{p}}}_{\text{T-TX}}$. Those vectors are used to compute the cost function $\xi(\mathbf{x})$ in Eq. (7). The vector $\hat{\bar{\mathbf{p}}}_{\text{T-TX}}$ that obtains the lowest value of $\xi(\mathbf{x})$ is used to compute the final target estimate using Eq. (10).

C. Nonlinearly Constrained Least Square Algorithms

The error minimizations of SI and SX algorithms do not view the problem as a whole. The SI algorithm disregards the nonlinear relationship of the entries of $\mathbf{x}$ ($\|\hat{\bar{\mathbf{p}}}_{\text{T-TX}\ell}\|$ should correspond precisely to $\hat{r}_{\text{TX}\ell\text{-T}}$). On the other hand, although the SX algorithm guarantees that $\|\hat{\bar{\mathbf{p}}}_{\text{T-TX}\ell}\| = \hat{r}_{\text{TX}\ell\text{-T}}$, it does not necessarily satisfy the identity in Eq. (6).

In [11], the NLCLS algorithm, defined for a scenario with M RXs and 1 TX, was proposed considering the complete mathematical problem in Eq. (6). By assuming all the constraints of the original nonlinear problem in Eq. (6), the resulting method enjoys some regularization effects that implicitly compensate target delay estimation errors. This section extends the NLCLS mathematical formulations to the generic case of M RXs and L TXs.

1) The NLCLS Method: We have L nonlinear constraint functions to satisfy the interdependence of the entries of $\mathbf{x}$ defined as

$$f_\ell(\mathbf{x}) = \mathbf{x}^\intercal \bar{\mathbf{I}}_\ell \mathbf{x} = 0, \quad \ell \in \mathcal{L}, \tag{13}$$

where the $L(N+1)\times L(N+1)$ matrix $\bar{\mathbf{I}}_\ell \triangleq \begin{bmatrix} \bar{\mathbf{I}}_\ell^{\text{top}} & \mathbf{0}_{LN\times L} \\ \mathbf{0}_{L\times LN} & \bar{\mathbf{I}}_\ell^{\text{bottom}} \end{bmatrix}$, $\bar{\mathbf{I}}_\ell^{\text{top}} = \begin{bmatrix} \mathbf{0}_{(\ell-1)N\times(\ell-1)N} & \mathbf{0}_{(\ell-1)N\times N} & \mathbf{0}_{(\ell-1)N\times(L-\ell)N} \\ \mathbf{0}_{N\times(\ell-1)N} & \mathbf{I}_{N\times N} & \mathbf{0}_{N\times(L-\ell)N} \\ \mathbf{0}_{(L-\ell)N\times(\ell-1)N} & \mathbf{0}_{(L-\ell)N\times N} & \mathbf{0}_{(L-\ell)N\times(L-\ell)N} \end{bmatrix}$, and the $L\times L$ matrix $\bar{\mathbf{I}}_\ell^{\text{bottom}}$ has all entries equal to zero, but the entry in row ℓ and column ℓ, which is equal to -1.

With the L constraints in Eq. (13), we can use L Lagrange multipliers λ_ℓ, $\ell \in \mathcal{L}$, and write $\nabla_{\mathbf{x}}\xi(\mathbf{x}) = \sum_{\ell=1}^{L} \lambda_\ell \nabla_{\mathbf{x}} f_\ell(\mathbf{x})$, which can be simplified to:

$$2\left(\mathbf{A}^\intercal\mathbf{A}\mathbf{x} - \mathbf{A}^\intercal\mathbf{z}\right) = 2\left(\sum_{\ell=1}^{L}\lambda_\ell\bar{\mathbf{I}}_\ell\right)\mathbf{x}. \tag{14}$$

As in [11] and [42], we use the Newton–Raphson method to solve Eq. (14). We define the unknown vector $\mathbf{v} = \begin{bmatrix}\hat{\mathbf{x}}^\intercal & \hat{\boldsymbol{\lambda}}^\intercal\end{bmatrix}^\intercal$, where $\hat{\boldsymbol{\lambda}} = \begin{bmatrix}\hat{\lambda}_1 \ldots \hat{\lambda}_L\end{bmatrix}^\intercal$. We then define vector $\mathbf{f}(\mathbf{v}) = \begin{bmatrix}\left(\nabla_{\mathbf{x}}\xi(\hat{\mathbf{x}}) - \sum_{\ell=1}^{L}\hat{\lambda}_\ell\nabla_{\mathbf{x}}f_\ell(\hat{\mathbf{x}})\right)^\intercal & f_1(\hat{\mathbf{x}}) & \ldots & f_L(\hat{\mathbf{x}})\end{bmatrix}^\intercal$, which, after some manipulation, leads to

$$\mathbf{f}(\mathbf{v}) = \begin{bmatrix} 2\left(\mathbf{A}^\intercal\mathbf{A}\hat{\mathbf{x}} - \mathbf{A}^\intercal\mathbf{z} - \sum_{\ell=1}^{L}\hat{\lambda}_\ell\bar{\mathbf{I}}_\ell\hat{\mathbf{x}}\right)^\intercal & \hat{\mathbf{x}}^\intercal\bar{\mathbf{I}}_1\hat{\mathbf{x}} \ldots \hat{\mathbf{x}}^\intercal\bar{\mathbf{I}}_L\hat{\mathbf{x}} \end{bmatrix}^\intercal. \tag{15}$$

The iterative process minimizes $\|\mathbf{f}(\mathbf{v}_k)\|$ updating $\mathbf{v}_k$ at each iteration k:

$$\mathbf{v}_{k+1} = \mathbf{v}_k - \mathbf{J}^{-1}(\mathbf{v}_k)\mathbf{f}(\mathbf{v}_k), \tag{16}$$

where $\mathbf{J}(\mathbf{v}_k)$ is the Jacobian of $\mathbf{f}$ evaluated at $\mathbf{v}_k$:

$$\mathbf{J}(\mathbf{v}_k) = \begin{bmatrix} 2(\mathbf{A}^\intercal\mathbf{A} - \sum_{\ell=1}^{L}[\hat{\lambda}_\ell]_k\bar{\mathbf{I}}_\ell) & -2\bar{\mathbf{I}}_1\hat{\mathbf{x}}_k & \ldots & -2\bar{\mathbf{I}}_L\hat{\mathbf{x}}_k \\ 2\hat{\mathbf{x}}_k^\intercal\bar{\mathbf{I}}_1 & 0 & \ldots & 0 \\ \vdots & \vdots & \vdots & \vdots \\ 2\hat{\mathbf{x}}_k^\intercal\bar{\mathbf{I}}_L & 0 & \ldots & 0 \end{bmatrix}. \tag{17}$$

The initial value $\mathbf{v}_0$ can be set to vector $\hat{\mathbf{x}}$ of the unconstrained LS solution as $\hat{\mathbf{x}}_0$, as defined in Eq. (8), and $[\hat{\boldsymbol{\lambda}}]_0 = \mathbf{0}_{L\times 1}$: $\mathbf{v}_0 = \begin{bmatrix}\left(\left(\mathbf{A}^\intercal\mathbf{A}\right)^{-1}\mathbf{A}^\intercal\mathbf{z}\right)^\intercal & \mathbf{0}_{L\times 1}^\intercal\end{bmatrix}^\intercal$.[2] The iterative procedure stops when $\|\mathbf{f}_k\| < \epsilon$, where ϵ represents the algorithm's tolerance.

2) Simplified Method: We propose here a faster and simplified version of the NLCLS (S-NLCLS). We start by observing that if Eq. (13) holds for all $\ell \in \mathcal{L}$ (i.e., $\|\bar{\mathbf{p}}_{\text{T-TX}\ell}\|$ corresponds exactly to $r_{\text{TX}\ell\text{-T}}$ for all $\ell \in \mathcal{L}$), then it follows that

$$\sum_{\ell=1}^{L}\|\bar{\mathbf{p}}_{\text{T-TX}\ell}\|^2 - \sum_{\ell=1}^{L} r_{\text{TX}\ell\text{-T}}^2 = 0. \tag{18}$$

The simplified algorithm is obtained by replacing the L constraints in Eq. (13) with a single nonlinear constraint function $f(\mathbf{x})$ that guarantees that Eq. (18) holds, i.e., $f(\mathbf{x}) = \mathbf{x}^\intercal\bar{\mathbf{I}}_{\text{c}}\mathbf{x} = 0$, where $\bar{\mathbf{I}}_{\text{c}} = \begin{bmatrix}\mathbf{I}_{NL\times NL} & \mathbf{0}_{NL\times L} \\ \mathbf{0}_{L\times NL} & -\mathbf{I}_{L\times L}\end{bmatrix}$.

To use this simplified scheme to minimize the model mismatch due to bistatic measurements in Eq. (6), we have $\nabla_{\mathbf{x}}\xi(\mathbf{x}) = \lambda\nabla_{\mathbf{x}}f(\mathbf{x})$, where λ is the Lagrange multiplier, that after some manipulation, leads to $2(\mathbf{A}^\intercal\mathbf{A}\mathbf{x} - \mathbf{A}^\intercal\mathbf{z}) = 2\lambda\bar{\mathbf{I}}_{\text{c}}\mathbf{x}$; which is solved, as in Section II-C1, iteratively using the Newton–Raphson method.

Similarly, we define vector $\mathbf{v} = \begin{bmatrix}\hat{\mathbf{x}}^\intercal & \hat{\lambda}\end{bmatrix}^\intercal$, vector

$$\mathbf{f}(\mathbf{v}) = \begin{bmatrix}\nabla_{\mathbf{x}}\xi(\hat{\mathbf{x}}) - \hat{\lambda}\nabla_{\mathbf{x}}f(\hat{\mathbf{x}}) \\ f(\hat{\mathbf{x}})\end{bmatrix} = \begin{bmatrix}2(\mathbf{A}^\intercal\mathbf{A}\hat{\mathbf{x}} - \mathbf{A}^\intercal\mathbf{z}) - 2\hat{\lambda}\bar{\mathbf{I}}_{\text{c}}\hat{\mathbf{x}} \\ \hat{\mathbf{x}}^\intercal\bar{\mathbf{I}}_{\text{c}}\hat{\mathbf{x}}\end{bmatrix}, \tag{19}$$

and matrix $\mathbf{J}(\mathbf{v}_k) = \begin{bmatrix}2(\mathbf{A}^\intercal\mathbf{A} - [\hat{\lambda}]_k\bar{\mathbf{I}}_{\text{c}}) & -2\bar{\mathbf{I}}_{\text{c}}\hat{\mathbf{x}} \\ 2\hat{\mathbf{x}}^\intercal\bar{\mathbf{I}}_{\text{c}} & 0\end{bmatrix}$. (20)

The initial value $\mathbf{v}_0$ can be set to $\hat{\mathbf{x}}_0$ as defined in Eq. (8), and $[\lambda]_0 = 0$: $\mathbf{v}_0 = \begin{bmatrix}\left(\left(\mathbf{A}^\intercal\mathbf{A}\right)^{-1}\mathbf{A}^\intercal\mathbf{z}\right)^\intercal & 0\end{bmatrix}^\intercal$.[3]

The NLCLS and S-NLCLS methods are summarized in Algorithm 1.

D. Computational Complexity

This work uses the Big $\mathcal{O}$ notation to tackle the computational complexity of algorithms [43]. Note that the product of an $n_{\text{r}}\times n_{\text{c}}$ matrix $\mathbf{M}_1$ and an $n_{\text{c}}\times n_{\text{c1}}$ matrix $\mathbf{M}_2$ has a complexity of $\mathcal{O}(n_{\text{r}}n_{\text{c}}n_{\text{c1}})$. Additionally, the inverse of $n_{\text{r}}\times n_{\text{r}}$ matrix $\mathbf{M}_3$ has a complexity of $\mathcal{O}(n_{\text{r}}^3)$.

For the SI algorithm, the dominant operation corresponds to the matrix multiplication in Eq. (8), whose computational complexity is $\mathcal{O}((N+1)^2L^3M)$.

As for the SX algorithm, and assuming we know the fixed positions of transmitters and receivers in the PCL system, we precompute $\mathbf{P}^\dagger = \left(\mathbf{P}_{\text{RX-TX}}^\intercal\mathbf{P}_{\text{RX-TX}}\right)^{-1}\mathbf{P}_{\text{RX-TX}}^\intercal$ offline. Consequently, the computational complexity for the SX method involves the following dominant operations:

- Computing Eq. (11) $2^L + 2$ times. Considering the final matrix-vector product as the dominant operation, the computational complexity is $\mathcal{O}((2^L+2)NL^2M)$.

[2] We use $[\hat{\boldsymbol{\lambda}}]_k$ to denote the estimated $\boldsymbol{\lambda}$, the Lagrange multiplier vector of the NLCLS algorithm, at iteration k, Moreover, we use $[\hat{\lambda}_\ell]_k$ to represent the estimated λ_ℓ, the ℓ-th element of $\hat{\boldsymbol{\lambda}}$, at iteration k.

[3] We use $[\hat{\lambda}]_k$ to represent the estimated λ, the Lagrange multiplier of the S-NLCLS algorithm, at iteration k.

Algorithm 1: Nonlinearly constrained least square methods (**NLCLS** and **S-NLCLS**)

Result: Estimated target position: $\hat{\mathbf{p}}_{\mathrm{T}}$

$k \leftarrow 0$ and $\hat{\mathbf{x}}_0 \leftarrow \left(\mathbf{A}^{\intercal}\mathbf{A}\right)^{-1}\mathbf{A}^{\intercal}\mathbf{z}$

; $[\hat{\boldsymbol{\lambda}}]_0 \leftarrow \mathbf{0}_{L\times 1}$ for NLCLS or $[\hat{\lambda}]_0 \leftarrow 0$ for S-NLCLS;

$\mathbf{v}_0 \leftarrow \begin{bmatrix}\hat{\mathbf{x}}_0 \\ [\hat{\boldsymbol{\lambda}}]_0\end{bmatrix}$ for NLCLS or $\mathbf{v}_0 \leftarrow \begin{bmatrix}\hat{\mathbf{x}}_0 \\ [\hat{\lambda}]_0\end{bmatrix}$ for S-NLCLS;

do

  $k = k + 1$;

  Update $\mathbf{J}(\mathbf{v}_k)$ using $\underbrace{\text{Eq. (17)}}_{\text{NLCLS}}$ or $\underbrace{\text{Eq. (20)}}_{\text{S-NLCLS}}$;

  Update $\mathbf{f}(\mathbf{v}_k)$ using $\underbrace{\text{Eq. (15)}}_{\text{NLCLS}}$ or $\underbrace{\text{Eq. (19)}}_{\text{S-NLCLS}}$;

  Update $\mathbf{v}_{k+1}$ using Eq. (16);

  $\hat{\mathbf{x}}_{k+1} \leftarrow$ first $(N+1)L$ entries of $\mathbf{v}_{k+1}$;

  $[\hat{\boldsymbol{\lambda}}]_{k+1} \leftarrow$ last L entries of $\mathbf{v}_{k+1}$ for NLCLS or $[\hat{\lambda}]_{k+1} \leftarrow$ last entry of $\mathbf{v}_{k+1}$ for S-NLCLS;

while $\|\mathbf{f}_k\| > \epsilon$;

$\hat{\tilde{\mathbf{p}}}_{\text{T-TX}} \leftarrow$ first NL entries of $\mathbf{v}_{k+1}$;

$\hat{\mathbf{p}}_{\mathrm{T}} = \left(\mathbf{I}_{\mathrm{a}}{}^{\intercal}\mathbf{I}_{\mathrm{a}}\right)^{-1}\mathbf{I}_{\mathrm{a}}{}^{\intercal}\left(\hat{\tilde{\mathbf{p}}}_{\text{T-TX}} + \mathbf{p}_{\mathrm{TX}}\right)$;

- Computing Eq. (7) 2^L times. The dominant operation in each computation is the matrix-vector product $\mathbf{Ax}$ such that the final complexity in the computational complexity corresponds to $\mathcal{O}(2^L ML^2(N+1))$.

The overall computational cost of the SX algorithm, considering the most significant operations, can be approximated as $\mathcal{O}((2^L+2)NL^2M + 2^L ML^2(N+1))$.

In both NLCLS and S-NLCLS algorithms, a numerical process iteratively compensates for measurement impairments to obtain a more accurate result. The dominant operation in each iteration involves the inversion of $\mathbf{J}(\mathbf{v}_k)$ in Eq. (17) for the NLCLS algorithm and Eq. (20) for the S-NLCLS algorithm. With K iterations taken into account, the most significant complexities of the numerical methods in NLCLS and S-NLCLS are, respectively, $\mathcal{O}(K(ML+L)^3)$ and $\mathcal{O}(K(ML+1)^3)$.

E. The Cramér-Rao Lower Bound

We consider a 3D PCL system whose positions of TXℓ, $\mathbf{p}_{\mathrm{TX}\ell} = \begin{bmatrix}x_{\mathrm{TX}\ell} & y_{\mathrm{TX}\ell} & z_{\mathrm{TX}\ell}\end{bmatrix}^{\intercal}$, $\ell \in \mathcal{L}$, and RXm, $\mathbf{p}_{\mathrm{RX}m} = \begin{bmatrix}x_{\mathrm{RX}m} & y_{\mathrm{RX}m} & z_{\mathrm{RX}m}\end{bmatrix}^{\intercal}$, $m \in \mathcal{M}$, are known and fixed. The unknown target location is $\mathbf{p}_{\mathrm{T}} = \begin{bmatrix}x_{\mathrm{T}} & y_{\mathrm{T}} & z_{\mathrm{T}}\end{bmatrix}^{\intercal}$.

One way to benchmark the estimation results is by employing the CRLB, which represents the lowest possible mean square error (MSE) of the optimal unbiased estimator. In our related PCL location problem, with multiple TXs, multiple RXs, and one target, the CRLB is a function of error variances of all bistatic range measurements, $\hat{r}_{\mathrm{B}m\ell}$, $m \in \mathcal{M}$, $\ell \in \mathcal{L}$. By applying Slepian-Bangs formula [44] and using all the available measurements in our target location problem, the $N \times N$ Fisher information matrix (FIM) can be expressed as $\mathbf{F} = \mathbf{G}^{\intercal}\mathbf{Q}_{\mathrm{B}}^{-1}\mathbf{G}$, where $\mathbf{Q}_{\mathrm{B}}$ is the $ML \times ML$ covariance matrix of the measurement errors impairing the $M \times L$ bistatic ranges, $r_{\mathrm{B}m\ell}$. $\mathbf{G} = \begin{bmatrix}\frac{\partial \mathbf{r}_{\mathrm{B}}}{\partial x_{\mathrm{T}}} & \frac{\partial \mathbf{r}_{\mathrm{B}}}{\partial y_{\mathrm{T}}} & \frac{\partial \mathbf{r}_{\mathrm{B}}}{\partial z_{\mathrm{T}}}\end{bmatrix}$ contains the partial derivatives with respect to the theoretical target position, where $\mathbf{r}_{\mathrm{B}} = \begin{bmatrix}\mathbf{r}_{\mathrm{B}1}^{\intercal} \dots \mathbf{r}_{\mathrm{B}L}^{\intercal}\end{bmatrix}^{\intercal}$ is the vector containing the theoretical (nominal) bistatic ranges, with $\mathbf{r}_{\mathrm{B}\ell} = \begin{bmatrix}r_{\mathrm{B}1\ell} \dots r_{\mathrm{B}mL}\end{bmatrix}^{\intercal}$. The appendix shows the mathematical formulations of the partial derivatives in matrix $\mathbf{G}$.

The CRLB is represented by the diagonal elements of the inverse of matrix $\mathbf{F}$. The MSE associated with the theoretical target location $\mathbf{p}_{\mathrm{T}}$, $\mathrm{MSE}_{\mathrm{T}}$, with N_{r} runs of the location algorithm, is defined as $\mathrm{MSE}_{\mathrm{T}} = \frac{1}{N_{\mathrm{r}}}\sum_{k=1}^{N_{\mathrm{r}}}\left\|\mathbf{p}_{\mathrm{T}} - \hat{\mathbf{p}}_{\mathrm{T}}^{(k)}\right\|^2$, where $\hat{\mathbf{p}}_{\mathrm{T}}^{(k)}$ is the k-th estimate of $\mathbf{p}_{\mathrm{T}}$. $\mathrm{MSE}_{\mathrm{T}}$ for an unbiased estimator is limited by CRLB as $\mathrm{MSE}_{\mathrm{T}} \geq \mathrm{tr}\left(\mathbf{F}^{-1}\right)$. Consequently, the root MSE (RMSE) associated with the theoretical target location,

$$\mathrm{RMSE}_{\mathrm{T}} = \sqrt{\mathrm{MSE}_{\mathrm{T}}}, \tag{21}$$

is limited by CRLB as $\mathrm{RMSE}_{\mathrm{T}} \geq \sqrt{\mathrm{tr}\left(\mathbf{F}^{-1}\right)}$.

III. Dealing with Outliers

The aforementioned location methods assume the knowledge of the bistatic range $r_{\mathrm{B}m\ell}$. In practice, this parameter is estimated, for instance, by using delay measurements, $\hat{\tau}_{m\ell}$, from the signals of each pair RXm–TXℓ: $\hat{r}_{\mathrm{B}m\ell} \triangleq c\hat{\tau}_{m\ell}$, where $c = 3 \times 10^8$ m/s represents the speed of light.

Line-of-sight blocking effect between the TX and target, or between target and RX, affects bistatic range estimations, creating much higher errors. Those abnormal values (i.e. mismeasurements) are considered outliers that must be tackled. It is worth mentioning that we do not consider detectable zero-Doppler clutter interference as outlier generators.

A. Cuboid-based Search Method

We propose a volumetric search method that can detect and remove outliers. In this case, eliminating mismeasurements and adapting the location algorithm to estimate the target position is necessary. This volumetric method also offers a direct target location estimate, which is particularly suitable when removing many outliers, and a valid location algorithm is not applicable due to a lack of data.

The proposed solution, cuboid-based search (CS) method, starts by partitioning the location region, $\mathcal{V} \subset \mathbb{R}^3$, into C_1 cuboids with dimensions $d_x^{(1)}$, $d_y^{(1)}$, and $d_z^{(1)}$.[4] The cuboids $\mathfrak{c}_i^{(1)}$, $i \in \mathfrak{C} \triangleq \{1, \dots, C_1\}$, form a partition of $\mathcal{V}$.

Each cuboid $\mathfrak{c}_i^{(1)}$ in $\mathcal{V}$ has a specific bistatic range interval associated with each RXm–TXℓ pair: $\mathcal{B}_{m\ell}^{i(1)} \triangleq \left[\min r_{\mathrm{B}m\ell}\left(\mathfrak{c}_i^{(1)}\right), \max r_{\mathrm{B}m\ell}\left(\mathfrak{c}_i^{(1)}\right)\right] \subset \mathbb{R}$, where $r_{\mathrm{B}m\ell}\left(\mathfrak{c}_i^{(1)}\right) \subset \mathbb{R}$ is the set of all RXm–TXℓ bistatic range nominal values for target locations in the cuboid $\mathfrak{c}_i^{(1)} \subset \mathcal{V}$. Geometrically, $\min r_{\mathrm{B}m\ell}\left(\mathfrak{c}_i^{(1)}\right)$ is related to the minimum bistatic range of the cuboid vertexes and $\max r_{\mathrm{B}m\ell}\left(\mathfrak{c}_i^{(1)}\right)$ is related to its maximum value. For each RXm–TXℓ pair, $m \in \mathcal{M}$ and $\ell \in \mathcal{L}$, a bistatic range $r_{\mathrm{B}m\ell}$, associated with a specific target location, $\mathbf{p}_{\mathrm{T}}$, belongs to a group of cuboids

[4] In this method, we use a superscript $\in \{1, 2\}$ in parenthesis to denote the first or second search.

that intersect the surface of an ellipsoid with foci associated with RXm and TXℓ and constant range difference $r_{m\ell}$.

The main principle underlying the CS method is to select the cuboid(s) that is intersected more times by the ellipsoids corresponding to the bistatic range measurements $\hat{r}_{\mathrm{B}m\ell}$, for all $m \in \mathcal{M}$ and $\ell \in \mathcal{L}$. The winner cuboid(s) represents the new search volume, which will be further split into smaller cuboids of dimensions $d_x^{(2)}$, $d_y^{(2)}$, and $d_z^{(2)}$, for which another cuboid selection is performed. This second search goes through a fine adjustment in the final process. The cuboid selected in this second search is called final cuboid. In case we have more than one winner cuboid as a result of the second search, we propose taking each cuboid's centroid as a possible target location to compute the cost function $\xi(\mathbf{x})$ in (7). The cuboid associated with the smallest cost is the final cuboid.

In any case, the final cuboid can classify consistent data as the bistatic measurements inside and outliers as the bistatic measurements outside the cuboid. On the other hand, the centroid of the selected cuboid gives us another target location estimate that does not depend on discarding outliers. Therefore, we name this direct estimate as CENTROID-CS. Algorithm 2 summarizes the CS method.

In terms of computational complexity, the dominant operation of the CS method is the initial exhaustive search within $\mathcal{V}$. The dominant operation is checking whether a bistatic range measurement falls within a predefined interval of a cuboid with complexity $\mathcal{O}(1)$. Considering the C_1 cuboids and ML bistatic measurements, we characterize the dominant computational complexity of the CS method as $\mathcal{O}(MLC_1)$.

Algorithm 2: Cuboid-based search (**CS**)

Result: outlier index pairs $(m,\ell) \in \mathcal{I}_{\mathrm{O}}$, non-outlier index pairs $(m,\ell) \in \mathcal{I}_{\mathrm{NO}}$, and centroid of final cuboid $p_{\bar{w}}^{\mathrm{cc}}$.

$\mathcal{Q} \leftarrow \mathcal{V}$ ▷ initialize the search volume;
for all $s \in \mathfrak{S} \triangleq \{1,2\}$ **do**
  Split $\mathcal{Q}$ into cuboids of sizes $\left(d_x^{(s)}, d_y^{(s)}, d_z^{(s)}\right)$;
  $i \in \mathfrak{C}_s \triangleq \{1,\ldots,C_s\}$ ▷ indexes of new cuboids $\mathfrak{c}_i^{(s)}$;
  for all $i \in \mathfrak{C}_s$ **do**
    $P_i^{(s)} \leftarrow 0$ ▷ initialize the counter per $\mathfrak{c}_i^{(s)}$;
  end
  for all $m \in \mathcal{M}$ **do**
    for all $\ell \in \mathcal{L}$ **do**
      for all $i \in \mathfrak{C}_s$ **do**
        $\mathcal{B}_{m\ell}^{i(s)} = \left[\min r_{\mathrm{B}m\ell}\left(\mathfrak{c}_i^{(s)}\right), \max r_{\mathrm{B}m\ell}\left(\mathfrak{c}_i^{(s)}\right)\right]$;
        if $\hat{r}_{\mathrm{B}m\ell} \in \mathcal{B}_{m\ell}^{i(s)}$ **then**
          $P_i^{(s)} \leftarrow P_i^{(s)} + 1$ ▷ add the counter;
        end
      end
    end
  end
  $\mathcal{W}_s \leftarrow \left\{ \underset{i \in \mathfrak{C}_s}{\operatorname{argmax}} P_i^{(s)} \right\}$ ▷ winner cuboid(s)' index;
  $\mathcal{Q} \leftarrow \mathfrak{c}_w^{(s)}, w \in \mathcal{W}_s$ ▷ new search volume;
end
$p_w^{\mathrm{cc}} \leftarrow$ center(s) of cuboid(s) of $\mathfrak{c}_w^{(2)}$, $w \in \mathcal{W}_2$;
$\xi^{(w)}(\mathbf{x}) \leftarrow$ cost(s) associated with p_w^{cc}, $w \in \mathcal{W}_2$;
$\bar{w} \leftarrow \left\{ \underset{w \in \mathcal{W}_2}{\operatorname{argmin}} \xi^{(w)}(\mathbf{x}) \right\}$;
$\mathfrak{c}_{\bar{w}}^{(2)} \leftarrow$ final winner cuboid;
$p_{\bar{w}}^{\mathrm{cc}} \leftarrow$ centroid of $\mathfrak{c}_{\bar{w}}^{(2)}$ (CENTROID-CS estimate);
$\mathcal{I}_{\mathrm{O}} \leftarrow \left\{ (m,\ell) \in \mathcal{M} \times \mathcal{L} \,|\, \hat{r}_{\mathrm{B}m\ell} \notin \mathcal{B}_{m\ell}^{\bar{w}(2)} \right\}$ ▷ outliers;
$\mathcal{I}_{\mathrm{NO}} \leftarrow \left\{ (m,\ell) \in \mathcal{M} \times \mathcal{L} \,|\, \hat{r}_{\mathrm{B}m\ell} \in \mathcal{B}_{m\ell}^{\bar{w}(2)} \right\}$ ▷ non-outliers.

B. Closest Neighbor Method

The proposed closest neighbor (CN) method discards outliers originated by target-RX NLoS and/or TX-target NLoS effects. This method detects and removes outliers in an iterative process where one outlier is detected in each iteration.

We start with an empty outlier index set $\mathcal{I}_{\mathrm{O}} = \emptyset$, and the non-outlier index set $\mathcal{I}_{\mathrm{NO}} = \mathcal{M} \times \mathcal{L}$ corresponding to all the available bistatic range measurements. Subsequently, the CN method establishes a list of candidates for most likely outliers in each iteration. To do that, we first define the normalized error of bistatic range, $\eta_{m\ell}$, for each RXm–TXℓ pair as

$$\eta_{m\ell} \triangleq \frac{\hat{r}_{\mathrm{B}_{m\ell}} - \bar{r}_{\mathrm{B}_{m\ell}}}{\bar{r}_{\mathrm{B}_{m\ell}}}, \tag{22}$$

in which $\bar{r}_{\mathrm{B}m\ell}$ is obtained from Eq. (1) by considering an estimated target location using all the measurements $\hat{r}_{\mathrm{B}m\ell}$ associated with indexes $(m,\ell) \in \mathcal{I}_{\mathrm{NO}}$. In case we have a mismeasurement due to the NLoS effect, $\hat{r}_{\mathrm{B}_{m\ell}}$ will likely be much greater than $\bar{r}_{\mathrm{B}_{m\ell}}$. Motivated by this fact, the candidates for outliers are then selected from the bistatic measurements $\hat{r}_{\mathrm{B}m\ell}$ associated with the index set $(m,\ell) \in \mathcal{I}_{\mathrm{NO}}$, when the normalized error $\eta_{m\ell}$ associated with the RXm–TXℓ pair follows the rule $\eta_{m\ell} > \mathrm{mean}(\eta_{m\ell})$. This mean value is computed across the measurements with indexes (m,ℓ) in the set $\mathcal{I}_{\mathrm{NO}}$.

For each candidate bistatic range measurement, we estimate the target position discarding all measurements associated with index pairs $(m,\ell) \in \mathcal{I}_{\mathrm{O}}$ and the candidate itself. This target position calculates the cost function $\xi(\mathbf{x})$ in (7). The candidate associated with the maximum cost is classified as an outlier; consequently, its index pair is included in the set $\mathcal{I}_{\mathrm{O}}$ and removed from the set $\mathcal{I}_{\mathrm{NO}}$.

The iterative process automatically stops when $\max|\eta_{m\ell}| < \alpha_{\mathrm{CN}}$, $(m,\ell) \in \mathcal{I}_{\mathrm{NO}}$, with α_{CN} being the threshold of the CN method that ensures that there is not a considerable difference between the bistatic ranges $\bar{r}_{\mathrm{B}_{m\ell}}$, computed employing the estimated target position, and consistent measurements $\hat{r}_{\mathrm{B}_{m\ell}}$. Algorithm 3 summarizes the CN method.

Regarding complexity, this method has to compute the cost function $\xi(\mathbf{x})$ and the target location estimate $\hat{\mathbf{p}}_{\mathrm{T}}$ many times. Moreover, for the SX algorithm, matrix $\mathbf{P}^{\dagger}$ cannot be precomputed offline due to its dynamic nature at each CN iteration and its computational load must be considered. The overall CS computational workload depends on the number of iterations and the quantity of candidate outliers per iteration.

Algorithm 3: Closest neighbor (**CN**)

Result: outlier index pairs $(m,\ell) \in \mathcal{I}_{\rm O}$, and non-outlier index pairs $(m,\ell) \in \mathcal{I}_{\rm NO}$.

$\mathcal{I}_{\rm O} \leftarrow \emptyset$, and $\mathcal{I}_{\rm NO} \leftarrow$ index pairs (m,ℓ) of all available $\hat{r}_{{\rm B}m\ell}, m \in \mathcal{M}, \ell \in \mathcal{L}$;
Estimate $\hat{\mathbf{p}}_{\rm T}$ using $\hat{r}_{{\rm B}m\ell}, \forall (m,\ell)$ pair $\in \mathcal{I}_{\rm NO}$;
Compute $\eta_{m\ell}$ as in Eq. (22) for all $\hat{r}_{{\rm B}m\ell} | (m,\ell)$ pairs $\in \mathcal{I}_{\rm NO}$;
while any $|\eta_{m\ell}| > \alpha_{\rm CN}$ **do**
  $\mathcal{I}_{\rm C} \leftarrow \{(m,\ell)$ pairs$|\eta_{m\ell} > {\rm mean}(\eta_{m\ell})\}$ ▷ candidate outlier index pairs;
  for all $\hat{r}_{{\rm B}m\ell} | (m,\ell)$pair $\in \mathcal{I}_{\rm C}$ **do**
    $\hat{\mathbf{p}}_{\rm T}^{(m\ell)} \leftarrow$ estimated $\hat{\mathbf{p}}_{\rm T}$ discarding measurements with index pairs in $\mathcal{I}_{\rm O}$ and $\hat{r}_{{\rm B}m\ell}$;
    $\xi^{(m\ell)}(\mathbf{x}) \leftarrow$ cost associated with $\hat{\mathbf{p}}_{\rm T}^{(m\ell)}$;
  end
  Add (m,ℓ) pair associated with $\max\left[\xi^{(m\ell)}(\mathbf{x})\right]$ to $\mathcal{I}_{\rm O}$;
  Exclude $\hat{\tau}_{m\ell}$ pair associated with $\max\left[\xi^{(m\ell)}(\mathbf{x})\right]$ from $\mathcal{I}_{\rm NO}$;
  Compute $\eta_{m\ell}$ as in Eq. (22) for all $\hat{r}_{{\rm B}m\ell} | (m,\ell)$ pairs $\in \mathcal{I}_{\rm NO}$;
  Estimate $\hat{\mathbf{p}}_{\rm T}$ discarding measurements with index pair in $\mathcal{I}_{\rm O}$;
end

IV. Target Location with Missing Measurements

The CS method offers a direct target location estimate (CS-CENTROID) that does not depend on outlier removal nor any special regard to missing measurements. However, when applying the CS/CN methods as selection techniques to discard outliers and/or a target not detected by one or more TX-RX pairs, PCL algorithms must be adapted to take missing measurements into account.

Let $\mathcal{I}_{\rm M}$ be the set of measurement index pairs (m,ℓ) associated with undetected measurements and $\mathcal{I}_{\rm O}$ be the set of measurement index pairs (m,ℓ) associated with outliers. We set the range differences associated with undetected measurements as zero to avoid unnecessary computation, $r_{m\ell} = 0, \forall\, (m,\ell) \in \mathcal{I}_{\rm M}$.

The location algorithms do not use the data associated with measurements, $\hat{r}_{{\rm B}m\ell}$ whose index pairs (m,ℓ) belong to the sets $\mathcal{I}_{\rm M}$ and $\mathcal{I}_{\rm O}$. Consequently, we have the following modifications:

1) In each matrix $\bar{\mathbf{P}}_{{\rm RX\text{-}TX}\ell}$, $\ell \in \mathcal{L}$, which is part of matrix $\mathbf{P}_{\rm RX\text{-}TX}$, remove the rows $\bar{\mathbf{p}}^{\mathsf{T}}_{{\rm RX}m\text{-}{\rm TX}\ell}$ whose TX/RX pairs are associated with index pairs $(m,\ell) \in \mathcal{I}_{\rm M} \cup \mathcal{I}_{\rm O}$.
2) In each vector $\mathbf{r}_\ell$, which is part of matrix $\mathbf{R}$, remove the rows $r_{m\ell}$ associated with index pairs $(m,\ell) \in \mathcal{I}_{\rm M} \cup \mathcal{I}_{\rm O}$.
3) In each vector $\mathbf{z}_\ell$, $\ell \in \mathcal{L}$, which is part of vector $\mathbf{z}$, remove the rows associated with index pairs $(m,\ell) \in \mathcal{I}_{\rm M} \cup \mathcal{I}_{\rm O}$.
4) In the set of selected pairs, $\mathcal{I}_{\rm S} \triangleq (\mathcal{M} \times \mathcal{L}) \setminus (\mathcal{I}_{\rm M} \cup \mathcal{I}_{\rm O})$, define the number of pairs with index ℓ as $\bar{M}_\ell$. In other words, $\bar{M}_\ell$ represents the number of selected consistent measurements per TXℓ.
5) In case $\bar{M}_\ell < N+1$ for SI, NLCLS and S-NLCLS, or $\bar{M}_\ell < N$ for SX, $\ell \in \mathcal{L}$, remove the columns associated with matrix $\bar{\mathbf{P}}_{{\rm RX\text{-}TX}\ell}$ in $\mathbf{P}_{\rm RX\text{-}TX}$, remove the column ℓ in matrix $\mathbf{R}$ and remove the rows associated with $\mathbf{z}_\ell$ in $\mathbf{z}$. In other words, in case we do not have enough measurements per TXℓ for a valid target location solution, remove all data associated with TXℓ.

In order to have a valid target location solution, we need at least one TXℓ, $\ell \in \mathcal{L}$, with enough selected consistent measurements. Formally, a valid target location solution may exist when there is at least one index $\ell \in \mathcal{L}$ for which $\bar{M}_\ell \geq N+1$ for SI, NLCLS and S-NLCLS, or $\bar{M}_\ell \geq N$ for SX. Otherwise, the location methods fail.

V. Experimental Results

This section begins by detailing the simulated multistatic PCL scenarios used in our experiments. Secondly, the section reports on the corresponding CRLB assessment. Then, the performance of the proposed location algorithms is described considering that all target delay measurements have been detected. Subsequently, we evaluate the effect of undetected measurements. Finally, the techniques to overcome mismeasurements (outliers) are evaluated.

A. Simulation Scenario

In [19], as mentioned in Section I, the authors proposed the EM-AR algorithm that models an unknown IoO signal as an autoregressive (AR) process to jointly estimate its temporal correlations and the passive radar parameters (delay and Doppler). They considered a bistatic PCL system whose SC in the receiver is contaminated by non-negligible noise, clutter, and DPI. In our experiments, we used as a reference the EM-AR MSEs of the target delay estimations reported in [19], Fig. 2a.

More specifically, given the sampling frequency $f_{\rm s}$ and the sampling interval $T_{\rm s} = \frac{1}{f_{\rm s}}$, the nominal PCL normalized parameters were as in [19], viz.: target delay $\tau = 28.89 T_{\rm s}$, Doppler frequency $f_{\rm D} = \frac{25.12 f_{\rm s}}{N_{\rm o}}$, with $N_{\rm o}$ representing the number of samples collected during the observation window, and clutter delay $\tau_{\rm c} = 10.24 T_{\rm s}$. The sampling frequency in SC and RC was such that $f_{\rm s} \geq 2\left(B_{\rm IoO} + f_{\rm D}^{(\max)}\right)$, with $B_{\rm IoO}$ corresponding to the incoming signal bandwidth and $f_{\rm D}^{(\max)}$ being the maximum detectable target Doppler.

Table I summarizes the experimental results (normalized target delay MSE) from [19] for the EM-AR algorithm.[5] This experiment assumed an ${\rm SNR_r} = 5$ dB in the RC , a DPI-to-noise ratio ${\rm DNR_s} = 10$ dB in the SC, a clutter-to-noise ratio ${\rm CNR_s} = 10$ dB in the SC, and varied the ${\rm SNR_s}$ in SC from -15 to 10 dB.

Our simulations considered 3D PCL scenarios with $M = 6$ RXs and $L \in \{1,2,3\}$ TXs. Each RX had one dedicated RC per TX with a directional antenna that received the IoO signals from each TX, and one dedicated SC antenna per TX pointing toward the surveyed area where the target was to be located.

[5] In [19], the sampling interval was set to $T_{\rm s} = 1$ s. In our experiment, we used $T_{\rm s} = 0.25$ μs.

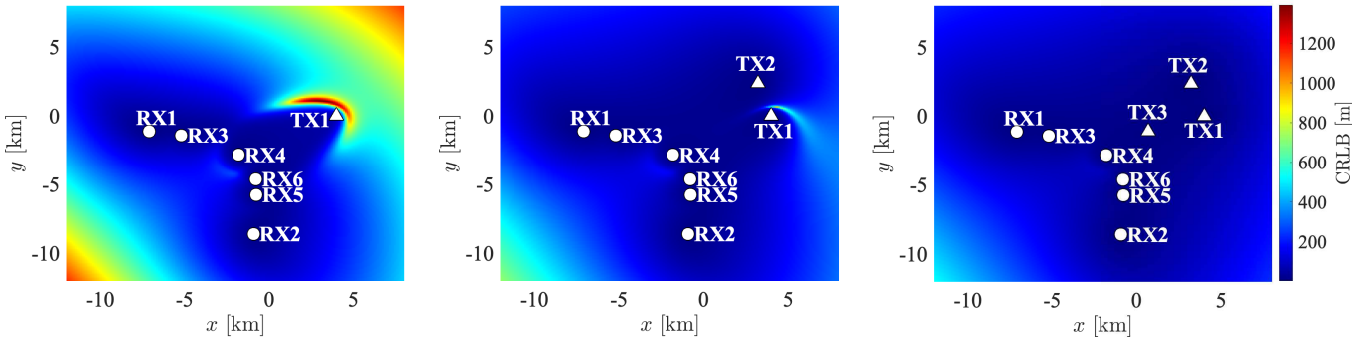

(a) 1 TX (b) 2 TXs (c) 3 TXs

Fig. 2. CRLB maps for PCL systems with 6 RXs and $L \in \{1, 2, 3\}$ TX(s).

TABLE I
NORMALIZED MSE MEASUREMENTS FROM [19]

SNR_S	-15 dB	-10 dB	-5 dB	0 dB	5 dB	10 dB
Normalized delay MSE	5.0	3.0	0.13	0.002	0.0006	0.0002
Delay RMSE [μs]	0.55902	0.43301	0.09014	0.01118	0.00612	0.00354
Bistatic RMSE [m]	167.71	129.90	27.04	3.35	1.84	1.06

TABLE II
POSITIONS (IN m) OF TXS AND RXS OF THE SIMULATED PCL SYSTEM

	RX1	RX2	RX3	RX4	RX5	RX6	TX1	TX2	TX3
x	-7112.11	-914.04	-5219.49	-1796.97	-756.53	-790.68	4000.00	3236.07	700.00
y	-1138.73	-8601.80	-1427.86	-2837.70	-5762.75	-4617.26	0.00	2351.14	-1100.00
z	61.12	78.13	70.60	31.80	48.24	88.39	176.72	111.71	143.50

The IoO signals of the different TXs covered the surveillance area but did not interfere with each other (e.g., FM signals of different radio stations). We assumed $f_\text{s} = 4$ MHz in SC and RC.

To be consistent with the MSEs obtained in [19], we used in our simulations a PCL geometry that guaranteed that the theoretical target delays were between 73% and 129% of the nominal target delay therein, $\tau = 28.89T_\text{s}$, that is $5.33 \leq \tau_{m\ell} \leq 9.32$ μs. The theoretical target location was $\mathbf{p}_{\text{T}1} = \begin{bmatrix}-2500 & -3700 & 421\end{bmatrix}^\intercal$ m. The positions of TXs and RXs were as in Table II.

B. CRLB Assessment

Fig. 2 shows the CRLB ($\sqrt{\text{tr}\,(\mathbf{F}^{-1})}$) maps for three multistatic PCL systems, whose positions of TXs and RXs are in Table II, in a square of 20×20 km^2 in the xy-coordinate plane at 421 m in the z-axis. The square is centered in $(x, y) = (-2, -2)$ km. We considered an additive impairment of the delay measurements, modeled as zero-mean Gaussian noise with standard deviation $\sigma_\tau = 0.020726733$ μs, or, equivalently, a standard deviation of the bistatic range noise, $\sigma_\text{B} = 6.218$ m, which corresponds to the CRLB $\sqrt{\text{tr}\,(\mathbf{F}^{-1})} = 100$ m, for the PCL system of 2 TXs (TX1 and TX2), 6 RXs (positions in Table II) and the target located at $\mathbf{p}_{\text{T}1}$. Therefore, $\mathbf{Q}_\text{B} = \sigma_\text{B}^2\mathbf{I}$.

The PCL system with one TX and 3 RXs (Fig. 2a) presents some target locations (high CRLB) with poor estimation precision, particularly behind TX1 and the RXs. When increasing the number of TXs (Fig. 2b and Fig. 2c), the precision in these locations improves, and the CRLB results of the PCL system with 3 TXs and 6 RXs are the best. The mean values of the CRLB results in Fig. 2a, Fig. 2b, and Fig. 2c were, respectively, 328.43, 143.11, and 95.12 m. A PCL system with more TXs and RXs tends to increase diversity and can exploit more measurements to achieve better target location estimations. We observed similar maps when experimenting with different altitudes.

C. Evaluation of Location Algorithms

A target of interest yields up to ML associated bistatic delay measurements $\hat{\tau}_{m\ell}$, $m \in \mathcal{M}$ and $\ell \in \mathcal{L}$. In this first experiment, we considered a target detection with probability of 1 for all TX-RX pairs and no outliers.

We assessed the PCL algorithms, described in Section II, in a multistatic PCL system with 2 TXs (TX1 and TX2) and 6 RXs. We used $N_\text{r} = 500$ independent runs of the algorithms to obtain the RMSE of the target location estimation $\mathbf{p}_{\text{T}1}$, RMSE_T, as defined in Eq. (21). Firstly, we disturbed each theoretical $\tau_{m\ell}$ associated with $\mathbf{p}_{\text{T}1}$ by adding zero-mean Gaussian noise with variances consistent with the MSE EM-AR results in [19]. The minimum variance of all $\tau_{m\ell}$ errors considered the minimum EM-AR MSE value of Table I ($\text{SNR}_\text{S} = 10$ dB) at $f_\text{s} = 4$ MHz, and the maximum variance was chosen taking as reference a CRLB value of 200 m at $\mathbf{p}_{\text{T}1}$ (approximately $\text{SNR}_\text{S} \approx$ -3 dB).

Fig. 3 shows the RMSE results for $\mathbf{p}_{\text{T}1}$. The S-NLCLS and NLCLS estimates outperformed the results of algorithms SI and SX. They approximated better the CRLB reference, especially in the z-axes, where the lack of diversity affected the location estimations. Moreover, we verified that the bias, $E\{\hat{\mathbf{p}}_{\text{T}1}\} - \mathbf{p}_{\text{T}1}$, was not significant in both x- and y-axes, considering distances in km. But in the z-axis, $\mathbf{p}_{\text{T}1}$ estimates presented a considerable bias (the bias decreases rapidly from -40 m) above $\sigma_\tau = 1.9 \times 10^{-2}\mu$s for the NLCLS and above $\sigma_\tau = 2.24 \times 10^{-2}\mu$s for the S-NLCLS.

Table III shows the computational complexity results of the location algorithms (Section II-D). This table also contains the mean runtime (in μs) when running the algorithms in an Apple MacBook Pro M1 with RAM of 16 GB. SI and SX algorithms are the least computationally demanding, although both S-NLCLS and NLCLS obtained good estimates in reasonable runtimes.

Fig. 4 shows the histograms of the Euclidean distance error of $\mathbf{p}_{\text{T}1}$ and $\mathbf{p}_{\text{T}2} = \begin{bmatrix}-2500 & -3700 & 1192\end{bmatrix}^\intercal$ m location

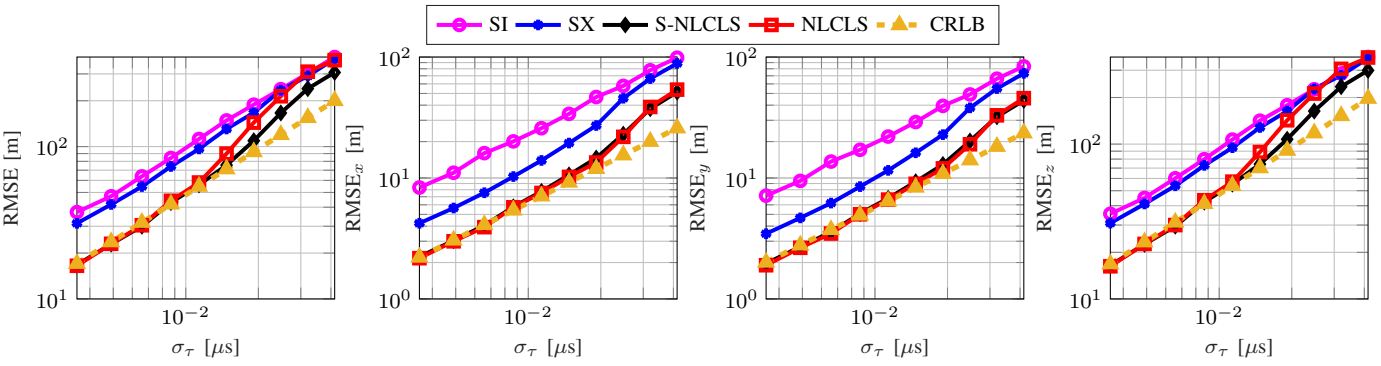

(a) 3D RMSE (b) x-axis RMSE (c) y-axis RMSE (d) z-axis RMSE

Fig. 3. RMSE of location estimates of $\mathbf{p}_{\mathrm{T}1}$ vs. standard deviation of delay measurement errors, σ_τ.

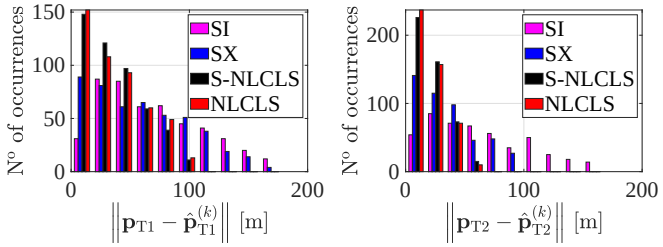

(a) $\mathbf{p}_{\mathrm{T}1}$ (b) $\mathbf{p}_{\mathrm{T}2}$

Fig. 4. Histogram of location estimation errors.

TABLE III
BIG $\mathcal{O}$ AND MEAN RUNTIME

Location algorithm	Complexity	mean runtime (ms)
SI	$\mathcal{O}(768)$	0.0138
SX	$\mathcal{O}(816)$	0.0470
S-NLCLS	$\mathcal{O}(21970)$	0.1684
NLCLS	$\mathcal{O}(27440)$	0.3326

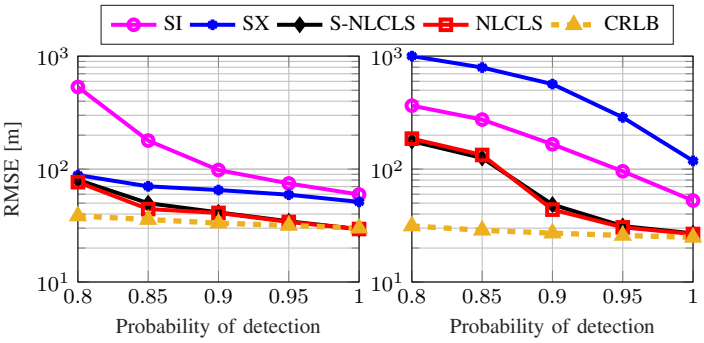

(a) $\mathbf{p}_{\mathrm{T}1}$ (b) $\mathbf{p}_{\mathrm{T}2}$

Fig. 5. RMSE vs. probability of target detection for 2 TXs and 6 RXs.

estimates when disturbing the theoretical target delays with zero-mean Gaussian error with a variance that corresponds to a CRLB $= 30$ m at $\mathbf{p}_{\mathrm{T}1}$. The variance was $\sigma_\tau^2 = 3.8664 \times 10^{-17}$ s^2 ($\sigma_{\mathrm{B}} = 1.865$ m and $\mathrm{SNR_S} = 4$ dB). The associated $\mathrm{RMSE_T}$ values for $\mathbf{p}_{\mathrm{T}1}$ were 61.13, 53.59, 29.65, and 29.30 m for SI, SX, S-NLCLS, and NLCLS algorithms. Moreover, The associated $\mathrm{RMSE_T}$ values for $\mathbf{p}_{\mathrm{T}2}$ were 51.87, 116.17, 26.39, and 25.87 m for SI, SX, S-NLCLS, and NLCLS algorithms. S-NLCLS and NLCLS obtained lower Euclidean errors.

D. Undetected Measurements

In a multistatic PCL scenario, some target delay measurements may not be detected – the IoO signal reflected by the target exists in the SC, but it is not identified. We evaluated here the effect of undetected measurements to estimate two distinct target positions ($\mathbf{p}_{\mathrm{T}1}$ and $\mathbf{p}_{\mathrm{T}2}$) considering 2 TXs (TX1 and TX2) and 6 RXs.

We assumed that each RX individually detects the target per SC and RC pair (individual detection per bistatic system). Some detection techniques that can be applied are in [1], [23]–[25]. Thus, our experiments considered no mismeasurements and a probability of detection, P_{D}, that varied from 0.8 to 1 in intervals of 0.5. For each P_{D}, $N_{\mathrm{r}} = 1000$ independent runs of the location algorithms were used to compute the RMSE as in Eq. (21). All theoretical $\tau_{m\ell}$ were disturbed with an error similar to the one used in the experiment of Section V-C.

For the location algorithms, we did the necessary modifications due to undetected measurements, and only valid modified solutions were used to compute the RMSE (Section IV). Our experiments had more than 98.9% of valid solutions in all P_{D} cases. Fig. 5 shows the RMSE results considering different probabilities of detection. Again, algorithms S-NLCLS and NLCLS attained better results, compensating for undetected measurements.

E. Mismeasurements

We emulated here outliers, usually present in bistatic range measurements due to NLoS (TX-target and/or target-RX) effects. This phenomenon is, in general, unavoidable in a practical passive radar system.

We assessed the proposed techniques to deal with outliers (Section III) in a simulated scenario with 3 TXs and 6 RXs (positions in Table II). In this experiment, we considered $N_{\mathrm{p}} = 27$ theoretical target locations, $\mathbf{p}_{\mathrm{T}n_{\mathrm{p}}} = \begin{bmatrix} x_{\mathrm{T}n_{\mathrm{p}}} & y_{\mathrm{T}n_{\mathrm{p}}} & x_{\mathrm{T}n_{\mathrm{p}}} \end{bmatrix}^{\mathsf{T}}$, $n_{\mathrm{p}} \in \{1, \ldots, N_{\mathrm{p}}\}$. It was supposed that the SC antennas (one per TX) in the RXs point toward the surveyed region where a target of interest can be located. The 27 locations corresponded to all combinations of $x_{\mathrm{T}n_{\mathrm{p}}}$, $y_{\mathrm{T}n_{\mathrm{p}}}$, and $z_{\mathrm{T}n_{\mathrm{p}}}$ taken from: $x_{\mathrm{T}n_{\mathrm{p}}} \in \{-8180, -2500, 3180\}$ m, $y_{\mathrm{T}n_{\mathrm{p}}} \in \{-9380, -3700, 2980\}$ m, and $z_{\mathrm{T}n_{\mathrm{p}}} \in \{421, 1192, 1693\}$ m.

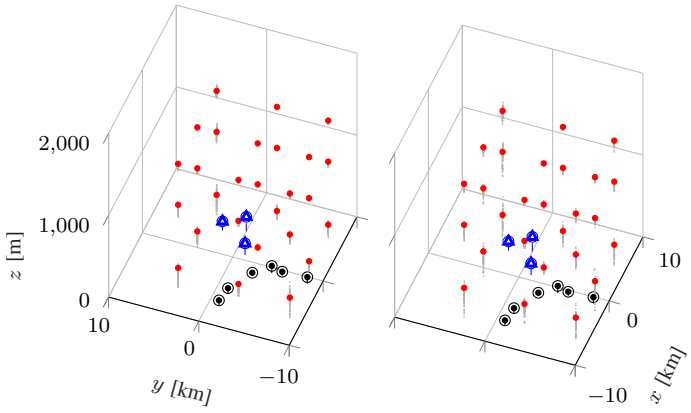

(a) LoS (b) 1 target-RX NLoS

Fig. 6. S-NLCLS-CS estimates of a target that can be located in 27 positions in a PCL system of 3 TXs and 6 RXs. TXs in blue, RXs in black, theoretical target positions in red, and estimates in grey. The axes of both plots follow the same scales and share the same labels.

TABLE IV
PCL LOCATION ALGORITHMS WHEN APPLYING DATA SELECTION

		Location algorithm			
		SI	**SX**	**NLCLS**	**S-NLCLS**
Selection techniques	**CS**	SI-CS	SX-CS	NLCLS-CS	S-NLCLS-CS
	CN	SI-CN	SX-CN	NLCLS-CN	S-NLCLS-CN

We executed $N_\mathrm{r} = 100$ independent runs on each of the 27 positions to calculate the RMSE, $\mathrm{RMSE}_{\mathrm{T}n_\mathrm{p}}$, $n_\mathrm{p} \in \{1,\ldots,N_\mathrm{p}\}$. To evaluate the location estimates in all possible theoretical positions where a target could be located, the global RMSE is defined as $\mathrm{RMSE}_\mathrm{G} = \sqrt{\frac{1}{N_\mathrm{p}}\sum_{n_\mathrm{p}=1}^{N_\mathrm{p}}\left[\mathrm{RMSE}_{\mathrm{T}n_\mathrm{p}}\right]^2}$. In our experiments, we applied the bistatic range measurement selection techniques (for the SI, SX, S-NLCLS, and NLCLS), as seen in Table IV. We also computed direct CENTROID-CS estimates.

We again simulated target delay impairments perturbing all $\tau_{m\ell}$ with a similar zero-mean Gaussian error used in Section V-C (results in Fig. 4) and Section V-D. To simulate the NLoS effect between a randomly selected TXℓ, $\ell \in \mathcal{L}$, and the target, we added a uniform random variable, distributed between 20% and 100% of the theoretical TXℓ-target range $r_{\mathrm{TX}\ell\text{-T}}$, to the bistatic range measurements $\hat{r}_{\mathrm{B}m\ell}$, $m \in \mathcal{M}$. Similarly, to simulate the NLoS effect between the target and a randomly selected RXm, a uniform random variable, distributed between 20% and 100% of the RXm-target range $r_{\mathrm{RX}m\text{-T}}$, was added to $\hat{r}_{\mathrm{B}m\ell}$, $\ell \in \mathcal{L}$. Any bistatic range measurement $\hat{r}_{\mathrm{B}m\ell}$ perturbed by TXℓ-target NLoS or/and target-RXm NLoS effects was considered a mismeasurement.

We considered different levels of NLoS, (number of target-RX NLoS, number of TX-target NLoS): (0,0), (1,0), (2,0), (0,1), (1,1), (3,0), and (2,1). The mentioned NLoS levels generated, respectively, 0, 3, 6, 6, 8, 9, and 10 outliers, out of a total of 18 bistatic range measurements.

When applying the CS method, the location region $\mathcal{V}$ had a volume $(20 \times 20 \times 2.4)$ km^3 $= 960$ km^3 and was limited in axes x, y, and z, respectively, by $-12 \le x \le 8$, $-12 \le y \le 8$, and $0 \le z \le 2.4$ km. This volume contained the 27 possible locations where the target could be located.

TABLE V
GLOBAL RMSE IN METERS FOR THE CS METHOD

		(Target-RX NLoS(s), TX-Target NLoS(s)) Number of mismeasurements						
		(0,0) 0	**(1,0) 3**	**(2,0) 6**	**(0,1) 6**	**(1,1) 8**	**(3,0) 9**	**(2,1) 10**
Case 1	**SI-CN**	**166.3**	**229.1**	3776.8	**238.7**	**311.5**	–	14834.9
	SX-CN	**92.4**	**146.9**	**460.0**	**240.9**	**227.8**	1499.5	**526.7**
	S-NLCLS-CN	**69.8**	**116.4**	**441.4**	**155.5**	**184.7**	–	752.4
	NLCLS-CN	**77.2**	**129.7**	**463.0**	**139.7**	**184.3**	–	756.2
	CENTROID-CS	**288.7**	**304.2**	**319.4**	**320.0**	**322.2**	**359.9**	**354.6**
Case 2	**SI-CN**	**166.2**	**226.6**	3909.6	**231.7**	**473.9**	–	13231.9
	SX-CN	**92.5**	**157.3**	**474.3**	**164.1**	**255.6**	1500.6	646.8
	S-NLCLS-CN	**65.9**	**122.6**	**447.6**	**134.7**	**230.6**	–	859.5
	NLCLS-CN	**73.8**	**144.9**	**471.4**	**135.4**	**226.8**	–	845.1
	CENTROID-CS	**268.7**	**275.6**	**327.5**	**302.7**	**330.9**	**407.7**	**500.6**
Case 3	**SI-CN**	**166.3**	**232.4**	6078.3	**224.5**	3518.5	–	20843.5
	SX-CN	**92.4**	**158.8**	**517.9**	**171.5**	**277.5**	1670.9	833.9
	S-NLCLS-CN	**69.8**	**126.5**	**515.7**	**127.7**	**398.2**	–	1282.9
	NLCLS-CN	**77.2**	**142.8**	**524.6**	**133.0**	**364.6**	–	1232.5
	CENTROID-CS	**201.2**	**230.8**	**292.7**	**267.8**	**317.3**	**445.3**	580.1

In our CS simulations, we tested cuboids of different sizes. Table V shows the global RMSE results, RMSE_G, for CS methods when using the following sizes for bigger and smaller cuboids, $(d_x^{(1)}, d_y^{(1)}, d_z^{(1)})$ and $(d_x^{(2)}, d_y^{(2)}, d_z^{(2)})$:

- case 1: $(150, 150, 150)$ m and $(75, 75, 75)$ m,
- case 2: $(200, 200, 200)$ m and $(100, 100, 100)$ m,
- case 3: $(300, 300, 200)$ m and $(150, 150, 100)$ m,

The above CS cases obtained better results, respectively, when $d_x^{(1)} = d_y^{(1)}$ =150, 200, and 300. When a location estimate was not possible to be obtained due to lack of consistent measurements, the corresponding entry in Table V contains the symbol "–". Highlighted RMSE results represent suitable location results (RMSE_G) considering the low diversity in the z-axis. For example, Fig. 6 shows S-NLCLS-CS estimates of a target that can be located in the previously mentioned 27 positions using the cuboid sizes of the case 3. Fig. 6a considers no target-RX and no TX-target NLoS (no outliers). Fig. 6b considers one target-RX NLoS and no TX-target NLoS (3 outliers).

For the CN method, we found the best threshold values by carrying out individual experiments, varying the thresholds between 0 and 0.7, and looking at the minimum global RMSE. The selected thresholds, α_CN, for SI-CN, SX-CN, S-NLCLS-CN, and NLCLS-CN were, respectively, 0.1, 0.075, 0.075, and 0.075. Table VI shows RMSE_G results considering the selected thresholds for CN methods. Highlighted entries show suitable location results.

In the results of Fig. 6 and in all the highlighted results of Table V and Table VI, one finds accurate target location estimates in the x- and y-axes (no bias in practice); however, due to the lack of diversity, typical inpractical PCL systems, the location estimates in z are more affected.

To verify the accuracy of the proposed selection techniques (Table IV), we also evaluated two crucial indicators: true positive rate (TPR) and false positive rate (FPR). TPR represents the probability that the bistatic range measurement is considered as an outlier when it indeed is an outlier. FPR

TABLE VI
BEST GLOBAL RMSE IN METERS FOR THE CN METHOD

	(Target-RX NLoS(s), TX-Target NLoS(s)) Number of mismeasurements						
	(0,0) 0	(1,0) 3	(2,0) 6	(0,1) 6	(1,1) 8	(3,0) 9	(2,1) 10
SI-CN	**164.4**	125463.3	428349.5	**231.0**	151098.2	–	435849.5
SX-CN	**97.0**	**439.3**	2450.6	**240.3**	**469.6**	11302.8	3239.9
S-NLCLS-CN	**74.5**	968.5	2677.8	**77.6**	1157.5	–	3101.1
NLCLS-CN	**82.6**	1335.3	2592.6	**89.8**	1772.3	–	3367.0

constitutes the probability that the bistatic range measurement is considered an outlier when it is not an outlier.

Fig. 7 shows TPR vs. number of Target-RX NLoS and Fig. 8 shows FPR vs. number of Target-RX NLoS. Comparing the RMSE results of Table V and Table VI with the TPR and FPR plots in Fig. 7 and Fig. 8, we see that, in general, the selection algorithms attain good $\mathrm{RMSE_G}$ results when TPR is high and FPR is low, as expected. However, in the simulated PCL system, we see that FPR has more influence on the accuracy of the final target location estimate (the presence of an outlier affects more than the absence of a consistent measurement). We can see this phenomenon comparing measurement selection for the case of one Target-RX NLoS and one TX-Target NLoS. SX-CN obtained $\mathrm{RMSE_G} = 469.60$ m with TPR = 0.994 and FPR = 0.093, and SX-CS method (case 2) obtained $\mathrm{RMSE_G} = 255.64$ m with TPR = 0.973 and FPR = 0.013.

Based on our numerical results, the proposed CS selection method overcame the outlier effects better than the CN methods. The effectiveness was demonstrated with lower $\mathrm{RMSE_G}$ values, higher TPR rates, and lower FPR rates. Outlier selection in CS does not depend on the location algorithm. The applied location methods helped us obtain better accuracy in the final location estimation. NLCLS-CS, S-NLCLS-CS and SX-CS (case 1, case 2 and case 3) obtained good estimates when overcoming up to 8 outliers out of a total of 18 measurements (one Target-RX NLoS and one TX-Target NLoS case).

On the other hand, CENTROID-CS, the selected cuboid's centroid, directly obtained reasonable estimates. This centroid estimates better the target location when increasing the number of outliers. CENTROID-CS does not depend on bistatic range measurement selection. Instead, it directly estimates the target location considering the volumetric location of the cuboid that intersects most of ellipsoids associated with most bistatic range measurements. CENTROID-CS cases 1 and 2 obtained good estimates when getting over up to 10 outliers out of a total of 18, and CENTROID-CS case 3 up to 9 outliers.

Regarding the computational load, in our PCL scenario, the CS method presented complexities of $\mathcal{O}(5.1{\times}10^6)$, $\mathcal{O}(2.2{\times}10^6)$ and $\mathcal{O}(9.6{\times}10^5)$, respectively, for cuboid sizes of case 1, case 2, and case 3. Moreover, the corresponding mean processing times were 241.91, 98.57, and 55.24 ms for CS cases 1, 2, and 3. The CN method presented complexities of $\mathcal{O}(7.1^4)$, $\mathcal{O}(7.8\times 10^5)$, $\mathcal{O}(5.6\times 10^5)$, and $\mathcal{O}(8.3\times 10^5)$, respectively, for SI-CN, SX-CN, S-NLCLS-CN, and NLCLS-CN. The corresponding mean processing times were 38.71, 95.89, 64.19, and 84.75 ms for SI-CN, SX-CN, S-NLCLS-CN, and NLCLS-CN.[6]

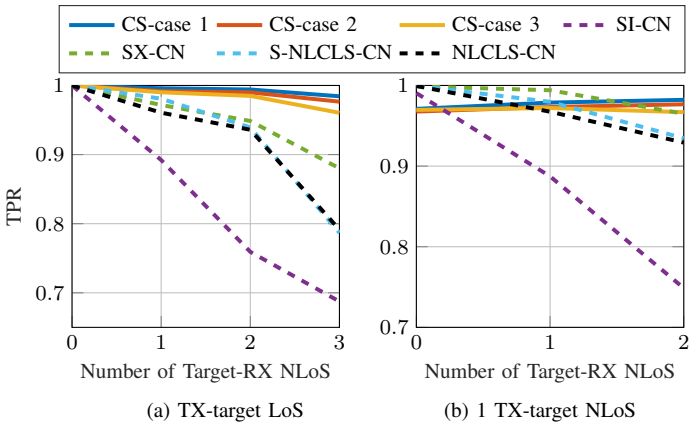

(a) TX-target LoS (b) 1 TX-target NLoS

Fig. 7. TPR vs. number of target-RX NLoS.

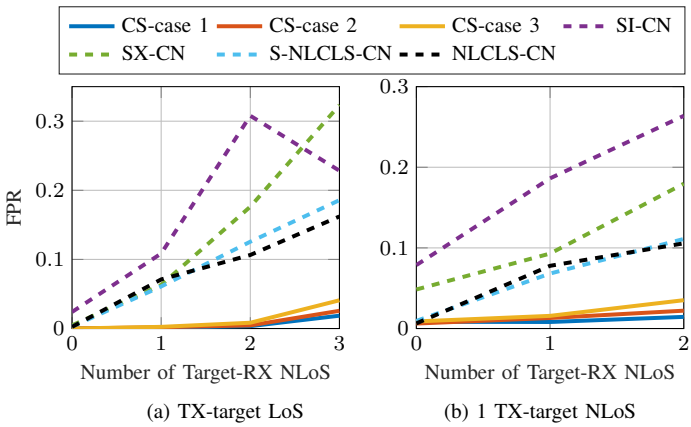

(a) TX-target LoS (b) 1 TX-target NLoS

Fig. 8. FPR vs. number of target-RX NLoS.

VI. CONCLUSION

This paper started by formulating the SI, SX, NLCLS and, S-NLCLS algorithms for PCL systems with multiple TXs/RXs systems and one target of interest. The NLCLS algorithm compensates bistatic measurement impairments with the help of constraints that take into account all the nonlinearities in the actual PCL problem. The proposed S-NLCLS algorithm is a faster version of the NLCLS algorithm that obtains accurate estimates using a single constraint.

This research work also contemplates mismeasurements generated by NLoS effect between target-RX and TX-target. We showed that applying the proposed measurement selection techniques (CS and CN) improves the accuracy of the target location. Numerical experiments also corroborated that high TPR and low FPR rates in the outliers' detection task lead to reasonable accuracy in the final estimation.

The best-performing proposed selection technique (CS) divides the location region into cuboids and discards the measurements outside the cuboids that most likely contain

[6]Big $\mathcal{O}$ complexity values are approximations regarding the actual computational complexity. We consider comparisons and products as dominant operations for CS and CN methods, respectively.

consistent measurements. CS outperforms CN, which iteratively removes outliers based on cost function comparisons.

The center of the selected cuboid in the CS method is considered another location estimation (CENTROID-CS). Hence, a significant contribution is that CENTROID-CS is a direct estimate that does not add computational load and does not depend on the outlier detection results. This estimate performs better than competing methods when increasing the number of outliers.

APPENDIX

PARTIAL DERIVATIVES IN CRLB

The partial derivative vectors of $\mathbf{G}$ are defined as follows

$$\frac{\partial \mathbf{r}_{\mathrm{B}}}{\partial x_{\mathrm{T}}} = \left[\left(\frac{\partial \mathbf{r}_{\mathrm{B}1}}{\partial x_{\mathrm{T}}}\right)^{\mathsf{T}} \ldots \left(\frac{\partial \mathbf{r}_{\mathrm{B}l}}{\partial x_{\mathrm{T}}}\right)^{\mathsf{T}} \ldots \left(\frac{\partial \mathbf{r}_{\mathrm{B}L}}{\partial x_{\mathrm{T}}}\right)^{\mathsf{T}}\right]^{\mathsf{T}}, \tag{A.1}$$

$$\frac{\partial \mathbf{r}_{\mathrm{B}}}{\partial y_{\mathrm{T}}} = \left[\left(\frac{\partial \mathbf{r}_{\mathrm{B}1}}{\partial y_{\mathrm{T}}}\right)^{\mathsf{T}} \ldots \left(\frac{\partial \mathbf{r}_{\mathrm{B}l}}{\partial y_{\mathrm{T}}}\right)^{\mathsf{T}} \ldots \left(\frac{\partial \mathbf{r}_{\mathrm{B}L}}{\partial y_{\mathrm{T}}}\right)^{\mathsf{T}}\right]^{\mathsf{T}}, \text{ and} \tag{A.2}$$

$$\frac{\partial \mathbf{r}_{\mathrm{B}}}{\partial z_{\mathrm{T}}} = \left[\left(\frac{\partial \mathbf{r}_{\mathrm{B}1}}{\partial z_{\mathrm{T}}}\right)^{\mathsf{T}} \ldots \left(\frac{\partial \mathbf{r}_{\mathrm{B}l}}{\partial z_{\mathrm{T}}}\right)^{\mathsf{T}} \ldots \left(\frac{\partial \mathbf{r}_{\mathrm{B}L}}{\partial z_{\mathrm{T}}}\right)^{\mathsf{T}}\right]^{\mathsf{T}}; \tag{A.3}$$

where

$$\frac{\partial \mathbf{r}_{\mathrm{B}l}}{\partial x_{\mathrm{T}}} = \left[\frac{\partial r_{\mathrm{B}1\ell}}{\partial x_{\mathrm{T}}} \quad \ldots \quad \frac{\partial r_{\mathrm{B}m\ell}}{\partial x_{\mathrm{T}}} \quad \ldots \quad \frac{\partial r_{\mathrm{B}m\ell}}{\partial x_{\mathrm{T}}}\right]^{\mathsf{T}}, \tag{A.4}$$

$$\frac{\partial \mathbf{r}_{\mathrm{B}l}}{\partial y_{\mathrm{T}}} = \left[\frac{\partial r_{\mathrm{B}1\ell}}{\partial y_{\mathrm{T}}} \quad \ldots \quad \frac{\partial r_{\mathrm{B}m\ell}}{\partial y_{\mathrm{T}}} \quad \ldots \quad \frac{\partial r_{\mathrm{B}m\ell}}{\partial y_{\mathrm{T}}}\right]^{\mathsf{T}}, \text{ and} \tag{A.5}$$

$$\frac{\partial \mathbf{r}_{\mathrm{B}l}}{\partial z_{\mathrm{T}}} = \left[\frac{\partial r_{\mathrm{B}1\ell}}{\partial z_{\mathrm{T}}} \quad \ldots \quad \frac{\partial r_{\mathrm{B}m\ell}}{\partial z_{\mathrm{T}}} \quad \ldots \quad \frac{\partial r_{\mathrm{B}m\ell}}{\partial z_{\mathrm{T}}}\right]^{\mathsf{T}}. \tag{A.6}$$

The bistatic target delay $r_{\mathrm{B}m\ell}$ can be expressed as $r_{\mathrm{B}m\ell} = r_{\mathrm{TX}\ell\text{-T}} + r_{\mathrm{RX}m\text{-T}} - r_{\mathrm{RX}m\text{-TX}\ell}$, $m \in \mathcal{M}$ and $\ell \in \mathcal{L}$. Therefore, its partial derivatives with respect to x_{T}, y_{T} and z_{T}, respectively, could be defined as

$$\frac{\partial r_{\mathrm{B}m\ell}}{\partial x_{\mathrm{T}}} = \frac{x_{\mathrm{T}} - x_{\mathrm{TX}\ell}}{r_{\mathrm{TX}\ell\text{-T}}} + \frac{x_{\mathrm{T}} - x_{\mathrm{RX}m}}{r_{\mathrm{RX}m\text{-T}}}, \tag{A.7}$$

$$\frac{\partial r_{\mathrm{B}m\ell}}{\partial y_{\mathrm{T}}} = \frac{y_{\mathrm{T}} - y_{\mathrm{TX}\ell}}{r_{\mathrm{TX}\ell\text{-T}}} + \frac{y_{\mathrm{T}} - y_{\mathrm{RX}m}}{r_{\mathrm{RX}m\text{-T}}}, \text{ and} \tag{A.8}$$

$$\frac{\partial r_{\mathrm{B}m\ell}}{\partial z_{\mathrm{T}}} = \frac{z_{\mathrm{T}} - z_{\mathrm{TX}\ell}}{r_{\mathrm{TX}\ell\text{-T}}} + \frac{z_{\mathrm{T}} - z_{\mathrm{RX}m}}{r_{\mathrm{RX}m\text{-T}}}. \tag{A.9}$$

ACKNOWLEDGMENT

This study was financed in part by the Coordenação de Aperfeiçoamento de Pessoal de Nível Superior (CAPES), Brazil – Finance code 001.

REFERENCES

[1] M. Malanowski, *Signal Processing for Passive Bistatic Radar*, 1st ed. Artech House, 2019.

[2] H. Griffiths and C. Baker, *An Introduction to Passive Radar*. Artech House, 2017.

[3] H. Griffiths and C. Baker, "Passive coherent location radar systems. Part 1: Performance prediction," *IEE Proceedings - Radar, Sonar and Navigation*, vol. 152, no. 3, pp. 153–159, Jun. 2005.

[4] P. Lingadevaru, B. Pardhasaradhi, and P. Srihari, "Feasibility of adopting 6g frequencies for transmitter of opportunity by passive radar," in *2022 IEEE International Symposium on Smart Electronic Systems (iSES)*, 2022, pp. 326–330.

[5] C. Oestges and F. Quitin, *Inclusive Radio Communications for 5G and Beyond*, 1st ed. Elsevier, 2021.

[6] R. S. Thomä, C. Andrich, G. D. Galdo, M. Dobereiner, M. A. Hein, M. Kaske, G. Schafer, S. Schieler, C. Schneider, A. Schwind, and P. Wendland, "Cooperative passive coherent location: A promising 5G service to support road safety," *IEEE Communications Magazine*, vol. 57, no. 9, pp. 86–92, Sep. 2019.

[7] P. Samczyński, K. Abratkiewicz, M. Płotka, T. P. Zieliński, J. Wszołek, S. Hausman, P. Korbel, and A. Ksieżyk, "5G Network-Based Passive Radar," *IEEE Transactions on Geoscience and Remote Sensing*, vol. 60, pp. 1–9, 2022.

[8] H. Kuschel, D. Cristallini, and K. E. Olsen, "Tutorial: Passive radar tutorial," *IEEE Aerospace and Electronic Systems Magazine*, vol. 34, no. 2, pp. 2–19, 2019.

[9] B. Pompeo, D. Nicolalde-Rodríguez, J. A. Apolinário Jr., M. Campos, and W. A. Martins, "Estimação de posição e velocidade de um alvo com base em TDOA e FDOA em sistemas de radar passivo usando redes neurais feedforward (in Portuguese)," in *Anais do XL Simpósio Brasileiro de Telecomunicações e Processamento de Sinais*. Sociedade Brasileira de Telecomunicações, 2022.

[10] D. P. Nicolalde-Rodríguez, W. A. Martins, J. A. Apolinário Jr., and L. P. Caloba, "Localização coerente passiva de um alvo usando redes neurais feedforward (in Portuguese)," *XXXIX Simpósio Brasileiro de Telecomunicações e Processamento de Sinais (SBrT 2021)*, Sep. 2021.

[11] D. P. Nicolalde-Rodríguez, J. A. Apolinário Jr., and W. A. Martins, "Robust passive coherent location via nonlinearly constrained least squares," *Latin American Symposium on Circuits and Systems (LASCAS 2021)*, Feb. 2021.

[12] M. Malanowski and K. Kulpa, "Two methods for target localization in multistatic passive radar," *IEEE Transactions on Aerospace and Electronic Systems*, vol. 48, no. 1, pp. 572–580, Jan. 2012.

[13] A. Aubry, A. D. V. Carotenuto, and L. Pallotta, "Joint exploitation of TDOA and PCL techniques for two-dimensional target localization," *IEEE Transactions on Aerospace and Electronic Systems*, vol. 56, no. 1, pp. 597–609, Feb. 2020.

[14] S. A. Kaiser, "Multistatic passive coherent location using the global position system," Ph.D. dissertation, The Pennsylvania State University - College of Engineering, 2017.

[15] L. Jinga, Z. Yongjuna, and L. Donghai, "Accurate single-observer passive coherent location estimation based on TDOA and DOA," *Chinese Journal of Aeronautics*, vol. 27, no. 4, pp. 913–923, Aug. 2014.

[16] S. Pak, B. Chalise, and B. Himed, "Target localization in multi-static passive radar systems with artificial neural networks," *International Radar Conference (RADAR)*, pp. 1–5, Sep. 2019.

[17] A. Dersan and Y. Tanik, "Passive radar localization by time difference of arrival," *IEEE Military Communications Conference (MILCOM)*, Oct. 2002.

[18] X. Zhang, H. Li, J. Liu, and B. Himed, "Joint delay and doppler estimation for passive sensing with direct-path interference," *IEEE Transactions on Signal Processing*, vol. 64, no. 3, pp. 630–640, 2016.

[19] F. Wang, H. Li, X. Zhang, and B. Himed, "Signal parameter estimation for passive bistatic radar with waveform correlation exploitation," *IEEE Transactions on Aerospace and Electronic Systems*, vol. 54, no. 3, pp. 1135–1150, 2018.

[20] M. Rashid and M. Naraghi-Pour, "Multitarget joint delay and doppler-shift estimation in bistatic passive radar," *IEEE Transactions on Aerospace and Electronic Systems*, vol. 56, no. 3, pp. 1795–1806, 2020.

[21] M. Rashid and M. Naraghi-Pour, "Multi-target delay and Doppler estimation in bistatic passive radar systems," in *2021 IEEE Radar Conference (RadarConf21)*, 2021, pp. 1–6.

[22] W. Xiong, J. Bordoy, C. Schindelhauer, A. Gabbrielli, G. Fischer, D. Schott, F. Hoeflinger, S. Rupitsch, and H. So, "Data–Selective Least Squares Methods for Elliptic Localization with NLOS Mitigation," *IEEE Sensors Letters*, vol. 5, no. 7, pp. 1–4, Jul. 2021.

[23] J. Liu, H. Li, and B. Himed, "On the performance of the cross-correlation detector for passive radar applications," *Signal Processing*, vol. 113, pp. 32–37, 2015.

[24] G. Cui, J. Liu, H. Li, and B. Himed, "Signal detection with noisy reference for passive sensing," *Signal Processing*, vol. 108, pp. 389–399, 2015.

[25] S. Gogineni, P. Setlur, M. Rangaswamy, and R. R. Nadakuditi, "Passive radar detection with noisy reference channel using principal subspace similarity," *IEEE Transactions on Aerospace and Electronic Systems*, vol. 54, no. 1, pp. 18–36, 2018.

[26] X. Zhang, H. Li, and B. Himed, "Multistatic detection for passive radar with direct-path interference," *IEEE Transactions on Aerospace and Electronic Systems*, vol. 53, no. 2, pp. 915–925, 2017.

[27] D. E. Hack, L. K. Patton, B. Himed, and M. A. Saville, "Detection in passive mimo radar networks," *IEEE Transactions on Signal Processing*, vol. 62, no. 11, pp. 2999–3012, 2014.

[28] H. Griffiths, "Chapter 16 - passive bistatic radar," in *Academic Press Library in Signal Processing: Volume 2*. Elsevier, 2014, vol. 2, pp. 813–855.

[29] J. E. Palmer and S. J. Searle, "Evaluation of adaptive filter algorithms for clutter cancellation in passive bistatic radar," in *2012 IEEE Radar Conference*, 2012, pp. 493–498.

[30] C. Moscardini, M. Conti, F. Berizzi, M. Martorella, and A. Capria, "Spatial adaptive processing for passive bistatic radar," in *2014 IEEE Radar Conference*, 2014, pp. 1061–1066.

[31] Y. Ma, T. Shan, Y. D. Zhang, M. G. Amin, R. Tao, and Y. Feng, "A novel two-dimensional sparse-weight nlms filtering scheme for passive bistatic radar," *IEEE Geoscience and Remote Sensing Letters*, vol. 13, no. 5, pp. 676–680, 2016.

[32] T. Peto and R. Seller, "Time domain filter comparison in passive radar systems," in *2017 18th International Radar Symposium (IRS)*, 2017, pp. 1–10.

[33] J. L. Garry, C. J. Baker, and G. E. Smith, "Evaluation of direct signal suppression for passive radar," *IEEE Transactions on Geoscience and Remote Sensing*, vol. 55, no. 7, pp. 3786–3799, 2017.

[34] W. Xiong, J. Liang, Z. Wang, and H. C. So, "Elliptic target positioning based on balancing parameter estimation and augmented lagrange programming neural network," *Digital Signal Processing*, vol. 136, p. 104004, 2023.

[35] W. Xiong, G. Cheng, C. Schindelhauer, and H. C. So, "Robust matrix completion for elliptic positioning in the presence of outliers and missing data," *IEEE Transactions on Geoscience and Remote Sensing*, vol. 61, pp. 1–12, 2023.

[36] W. Xiong and H. C. So, "Outlier-robust passive elliptic target localization," *IEEE Geoscience and Remote Sensing Letters*, vol. 20, pp. 1–5, 2023.

[37] D. B. Haddad, W. A. Martins, L. W. P. Biscainho, M. V. M. Costa, and K. Kim, "Choosing coherent times of flight for improved acoustic sensor localization," *International Telecommunications Symposium (ITS 2014)*, Aug. 2014.

[38] D. B. Haddad, M. V. S. Lima, W. A. Martins, L. W. P. Biscainho, L. O. Nunes, and B. Lee, "Acoustic sensor self-localization: Models and recent results," *Wireless Acoustic Sensor Networks and Applications*, vol. 2017, Oct. 2017.

[39] J. A. Apolinário Jr., H. Yazdanpanah, A. S. Nascimento, and M. L. R. de Campos, "A Data-selective LS Solution to TDOA-based Source Localization," *IEEE International Conference on Acoustics, Speech and Signal Processing (ICASSP 2019)*, Apr. 2019.

[40] I. L. Freire, P. C. Prandel, and J. A. Apolinário Jr., "Sobre a escolha de sinais em arranjos de microfones estimando DoA com GCC-PhaT - in Portuguese," *XXX Simpósio Brasileiro de Telecomunicações (SBrT 2012)*, Sep. 2012.

[41] I. L. Freire, "Robust direction-of-arrival by matched-lags, applied to gunshots," *The Journal of the Acoustical Society of America*, vol. 135, no. 6, pp. 246–251, Jun. 2014.

[42] J. G. C. Ribeiro, F. G. Serrenho, J. A. Apolinário Jr., and A. L. L. Ramos, "Improved DoA estimation with application to bearings-only acoustic source localization," in *IEEE International Symposium on Signal Proc. and Information Technology (ISSPIT 2017)*, Dec. 2017, pp. 100–105.

[43] M. Sipser, *Introduction to the Theory of Computation*, 3rd ed. Cengage Learning, 2013.

[44] H. L. Trees, *Classical Detection and Estimation Theory*. John Wiley and Sons, Ltd, 2001, ch. 2, pp. 19–165.

Daniel Patricio Nicolalde Rodríguez (IEEE Student Member and SBrT Student Member) received Telecommunications Engineering degree from Escuela Politécnica del Ejército (ESPE, Quito, Ecuador, in 2007) and the M.Sc. degree in Electrical Engineer (EE) from the Military Institute of Engineering (IME, Rio de Janeiro, Brazil, in 2010). He has been working as Telecommunications Consultant, in the field of IP/MPLS and mobile networks. Currently, Daniel is a Ph. D. student with the Program of Electrical Engineering of the Federal University of Rio de Janeiro (UFRJ, Rio de Janeiro, Brazil). His main research areas are DSP and applications.

Wallace A. Martins (Senior Member, IEEE) is a Full Professor at ISAE-SUPAERO, Université de Toulouse, France. All his degrees in Electrical Engineering were obtained from UFRJ, Brazil. He worked as a researcher at the University of Luxembourg from 2019 to 2023 and was an Associate Professor at UFRJ from 2013 to 2022. He is an Associate Editor for IEEE SIGNAL PROCESSING LETTERS and EURASIP Journal on Advances in Signal Processing. Prof. Martins has been awarded the Best Student Paper at EUSIPCO-2009 and the 2011 Best Brazilian D.Sc. Dissertation from Capes. His research mainly focuses on signal processing and wireless and satellite communications.

José Antonio Apolinário Jr. (IEEE Senior Member and SBrT Senior Member) graduated from the Military Academy of Agulhas Negras in 1981 and received the following degrees: B.Sc.-EE from the Military Institute of Engineering (IME), in 1998, M.Sc.-EE from the University of Brasília, in 1993, and D.Sc.-EE from the Federal University of Rio de Janeiro, in 1998. He is currently a Professor at IME, where he has already served as Head of Department and Vice-Rector for Study and Research. He was a Visiting Professor at the Escuela Politécnica del Ejército (ESPE, Ecuador), from 1999 to 2000, and a Visiting Professor (2004 and 2006) at Helsinki University of Technology (now Aalto University, Finland). He founded and was the first Chair of the Rio de Janeiro Communications Society Chapter. His research interests comprise many aspects of DSP, including adaptive filtering, acoustics, and array signal processing.

Marcello L. R. de Campos (Senior Member, IEEE) received the Engineering (cum laude) degree from the Federal University of Rio de Janeiro (UFRJ), Rio de Janeiro, Brazil, in 1990, the M.Sc. degree from COPPE/UFRJ in 1991, and the Ph.D. degree from the University of Victoria, Victoria, BC, Canada, in 1995, all in Electrical Engineering. Since 1998 he has been Professor with the Electrical Engineering Program, COPPE/UFRJ, having served as Vice-Chair and Chair in 2004 and 2005, respectively. He is currently serving a four-year term as Vice-Director for COPPE. His research interests include adaptive signal processing in general and its application to distributed networks, in particular, adaptive beamforming, statistical signal processing, signal processing for communications, underwater, mobile and wireless communications, and MIMO systems. He served as the IEEE Communications Society Regional Director for Latin America in 2000 and 2001, Local-Arrangements Co-Chair for GLOBECOM99, Finance Chair for SPAWC 2008, Plenary Chair for ISCAS 2011, and Technical Co-Chair for the 2013 Brazilian Telecommunications Symposium. He founded and was Chair of the IEEE Signal Processing Society Rio de Janeiro Chapter from 2011 to 2017. He is the current Chair of the Visibility & Outreach Committee of the Signal Processing Society Education Board.